MID-AMERICA TRANSPORTATION CENTER

Report # MATC-UNL: 004-45

Final Report

WBS: 25-1121-0005-004-45

Assessing Performance of Geosynthetic Reinforced Pavement with a Large-Scale Tracking Wheel Test and Dynamic Cone Penetrometer

Jongwan Eun, PhD, PE
Associate Professor
Department of Civil and Environmental Engineering
University of Nebraska-Lincoln

Seunghee Kim, PhD, PE
Associate Professor

Chung R Song, PhD, AE, M ASCE
Associate Professor

Jinying Zhu, PhD
Professor

Daniel Robertson
Graduate Research Assistant

Yusuf Alhowaidi
Graduate Research Assistant

Hung Van
Graduate Research Assistant

Laith Ibdah
Graduate Research Assistant

Kenaz Owusu
Graduate Research Assistant

2024

A Cooperative Research Project sponsored by U.S. Department of Transportation- Office of the Assistant Secretary for Research and Technology

Assessing Performance of Geosynthetic Reinforced Pavement with a Large-Scale Tracking Wheel Test and Dynamic Cone Penetrometer

Jongwan Eun, Ph.D, P.E.
PI
Associate Professor
Civil and Environmental Engineering Department

Seunghee Kim, Ph.D, P.E.
Co-PI
Associate Professor
Civil and Environmental Engineering Department

Chung R. Song, Ph.D. AE, M. ASCE
Co-PI
Associate Professor
Civil and Environmental Engineering Department

Jinying Zhu, PhD
Co-PI
Professor
Civil and Environmental Engineering Department

Daniel Robertson
Graduate Research Assistant
Civil and Environmental Engineering Department

Yusuf Alhowaidi
Graduate Research Assistant
Civil and Environmental Engineering Department

Hung Van
Graduate Research Assistant
Civil and Environmental Engineering Department

Laith Ibdah
Graduate Research Assistant
Civil and Environmental Engineering Department

Kenaz Owusu
Graduate Research Assistant
Civil and Environmental Engineering Department

A Report on Research Sponsored by Nebraska Department of Transportation

Mid-America Transportation Center

University of Nebraska–Lincoln

February 2024

Technical Report Documentation Page

1. Report No. 25-1121-0005-004-45	2. Government Accession No.	3. Recipient's Catalog No.
4. Title and Subtitle Assessing Performance of Geosynthetic Reinforced Pavement with a Large-Scale Tracking Wheel Test and Dynamic Cone Penetrometer		5. Report Date February 2024
		6. Performing Organization Code
7. Author(s) Jongwan Eun, Seunghee Kim, Chung R. Song, Jinying Zhu, Daniel Robertson, Yusuf Alhowaidi, Hung Van , Laith Ibdah, Kenaz Owusu		8. Performing Organization Report No. 25-1121-0005-004-45
9. Performing Organization Name and Address University of Nebraska-Lincoln Department of Civil and Environmental Engineering Peter Kiewit Institute 200E 1110 South 67th St Omaha, NE 68182-0178 Mid-America Transportation Center 2200 Vine St Lincoln, NE 68583-0851		10. Work Unit No. (TRAIS)
		11. Contract or Grant No. 69A3551747107
12. Sponsoring Agency Name and Address Nebraska Department of Transportation Research Section 1400 Hwy 2 Lincoln, NE 68502		13. Type of Report and Period Covered Final Report
		14. Sponsoring Agency Code MATC TRB RiP No. 91994-76
15. Supplementary Notes		

16. Abstract

This study presents an evaluation of geosynthetic reinforced pavements using the Large-Scale Tracking Wheel (LSTW) Test. The performance of geosynthetic reinforced pavement layer was assessed under rolling wheel loading which replicates the real-world traffic loading scenario. The parameters assessed included the permanent deformation (rutting), strength/stiffness change and pressure reduction effects at the pavement layer interface. Results from this research indicated that geosynthetic placed at the interface of the subgrade/base layer led to improvement in pavement strength/stiffness, as observed through the Dynamic Cone Penetrometer (DCP) Index and Resilient Modulus Results. A reduction in permanent deformation, commonly known as rutting was obtained for the geosynthetic reinforced case as well. Additionally, the pressure exerted on the subgrade layer also reduced with the application of geosynthetics between the subgrade/base layers. This notable reduction in pressure on the subgrade highlights the crucial role of geosynthetic reinforcement in distributing loads more evenly within the pavement structure, thereby enhancing its longevity and durability. Employing numerical modeling with parameters obtained from laboratory tests, simulations of practical pavement layers were conducted for different scenarios involving different geosynthetic types and positions. Results of these simulations showed a reduction in settlement and vertical stress for geosynthetic reinforced cases as compared with unreinforced cases. These simulations affirmed the findings of the large-scale tests as well.

17. Key Words Geosynthetics, subgrade, numerical modeling, pullout test, direct shear test, dynamic cone penetrometer test, large-scale tracking wheel	18. Distribution Statement		
19. Security Classif. (of this report) Unclassified	20. Security Classif. (of this page) Unclassified	21. No. of Pages 82	22. Price

Table of Contents

List of Figures

List of Tables

Disclaimer

The contents of this report reflect the views of the authors, who are responsible for the facts and the accuracy of the information presented herein. The contents do not necessarily reflect the official views or policies neither of the Nebraska Department of Transportation nor the University of Nebraska-Lincoln. This report does not constitute a standard, specification, or regulation. Trade or manufacturers' names, which may appear in this report, are cited only because they are considered essential to the objectives of the report.

The United States (U.S.) government and the State of Nebraska do not endorse products or manufacturers. This material is based upon work supported by the Federal Highway Administration under SPR-P1(see your contract for this #. Any opinions, findings and conclusions or recommendations expressed in this publication are those of the author(s) and do not necessarily reflect the views of the Federal Highway Administration."

Abstract

This study presents an evaluation of geosynthetic reinforced pavements using the Large-Scale Tracking Wheel (LSTW) Test. The performance of geosynthetic reinforced pavement layer was assessed under rolling wheel loading which replicates the real-world traffic loading scenario. The parameters assessed included the permanent deformation (rutting), strength/stiffness change and pressure reduction effects at the pavement layer interface. Results from this research indicated that geosynthetic placed at the interface of the subgrade/base layer led to improvement in pavement strength/stiffness, as observed through the Dynamic Cone Penetrometer (DCP) Index and Resilient Modulus Results. A reduction in permanent deformation, commonly known as rutting was obtained for the geosynthetic reinforced case as well. Additionally, the pressure exerted on the subgrade layer also reduced with the application of geosynthetics between the subgrade/base layers. This notable reduction in pressure on the subgrade highlights the crucial role of geosynthetic reinforcement in distributing loads more evenly within the pavement structure, thereby enhancing its longevity and durability. Employing numerical modeling with parameters obtained from laboratory tests, simulations of practical pavement layers were conducted for different scenarios involving different geosynthetic types and positions. Results of these simulations showed a reduction in settlement and vertical stress for geosynthetic reinforced cases as compared with unreinforced cases. These simulations affirmed the findings of the large-scale tests as well.

Chapter 1 Introduction

1.1 Introduction

The structural paradigm of road design, traditionally characterized by a surface layer, base layer, and subgrade layer, witnessed a transformative shift in 1926 with the pioneering efforts of the South Carolina Highway Department in integrating geosynthetics into low-volume roadway construction (Koerner et al., 1997). By the mid-1970s, there was an increase in technical papers about geosynthetics and their applications, leading to the development of geosynthetic design methodologies for low-volume rural forest roads by the U.S. Department of Agriculture Forest Service (USFS) using a trial-and-error basis. This resulted in one of the first guidelines for fabric construction and maintenance for unpaved roads in the US, as detailed in the finalized report by Steward et al. (1977). The improvement of road layers through the utilization of geosynthetic materials has been investigated and proven by numerous researchers. A geotextile-reinforced pavement layer exhibits reduced vertical deflection, delayed surface cracking, as well as a reduction in the horizontal movement of granular material. Additionally, it results in increased stiffness and an increase in the load-carrying capacity for the subgrade (Al-Qadi et al. 2011, Zofka et al., 2017, Zornberg, 2017 and Zumrawi and Abdalgadir, 2019).

Geosynthetic-reinforced soil has some limitations to evaluate on the lab scale, including scale effects and cyclic rolling loads. This study aims to modify large-scale tests to replicate rolling loads and evaluate the performance of geosynthetic reinforced road pavement layers.

1.2 Problem Statement

Geosynthetics reinforcement such as geogrid, geotextile, etc. has been used as a viable alternative to stabilize the base and subgrade of roadway pavement construction in regions with soft and/or problematic subgrade (foundation) soils (Groud 2004; Holtz et al. 2008; Eun et al. 2017; Kaswell 1963; Haliburton et al. 1980; Myles and Carswell 1986; and Koerner 2005). Geosynthetics is marketed as a viable alternative to traditional pavement systems, with the ability to reduce construction costs while maintaining equivalent structural performance. The benefits of using geosynthetics include improved pavement durability and reduced maintenance requirements (**Figure 1.1**). Despite the potentially higher initial construction cost compared to traditional methods, geosynthetics yield a lower overall life cycle cost by minimizing maintenance requirements and enhancing pavement durability (Barksdale et al. 1989; Zornberg, 2010; Koerner 2012; Christopher 2014; and Zornberg 2017).

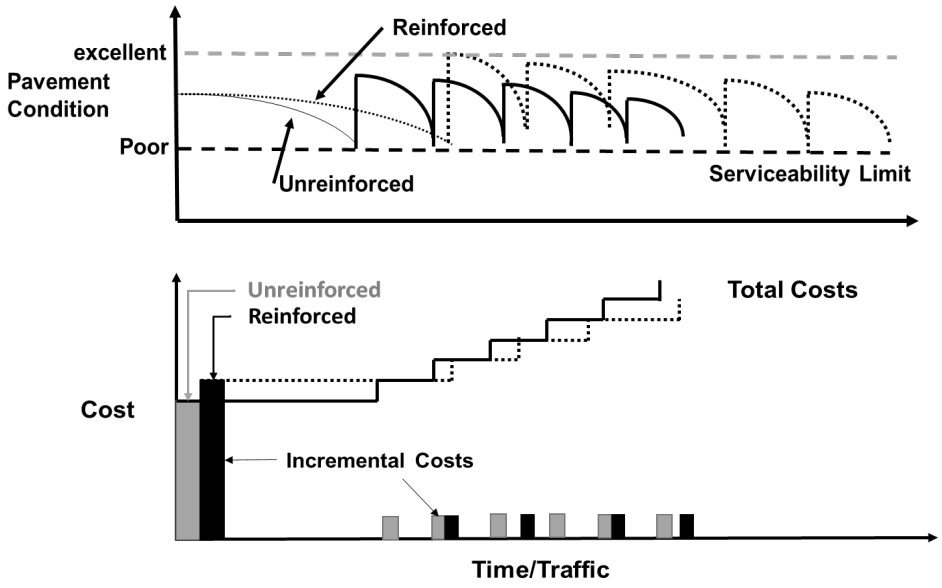

Figure 1.1 Conceptual illustration of life-cycle cost for reinforced and unreinforced pavements (adapted from Perkins et. al, 2004).

The key idea behind a geosynthetic is its ability to redistribute vehicle load, which in turn, is a redistribution of stress in the pavement structure. The stress distribution is reallocated in the horizontal direction along the geosynthetic (**Figure 1.2**). The horizontal tensile strains are reduced as the confinement and interlocking between layers are intensified (Zornberg 2017).

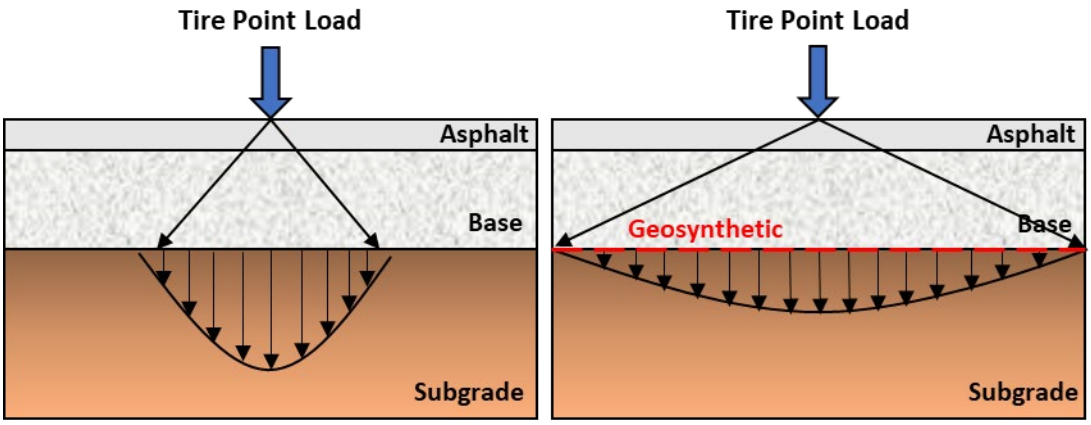

Figure 1.2 Cross-sectional roadway showing load distribution with and without geosynthetics (modified from Zornberg and Gupta, 2010).

There have been several studies that have investigated the effects of geosynthetics under flexible pavements. Nonetheless, only a handful of states have implemented this technique, presumably due to the lack of familiarity with this product among contractors and state departments and the initial cost increase. Though the Federal Highway Administration (FHWA) published a reference manual for its design and construction in 2008, which showed a general procedure for properly applying geosynthetics in roadway design with different California Bearing Ratio (CBR) values for soils, there are still some uncertainties regarding region-specific material properties and the types of geosynthetic products to calibrate the design process accurately. It is evident there has been limited research conducted to identify the performance evaluation of geosynthetics for different soil types in Nebraska. Consequently, there are no current well-defined provisions in the Nebraska Department of Transportation (NDOT) Standard Specifications for Highway Construction regarding geosynthetic reinforcement design for roadway systems.

1.3 Objective Statement

This proposed research aims to achieve three primary objectives:

(1) Develop a large-scale track wheel (LSTW) test with multiple non-destructive testing sensors to assess the performance of geosynthetic-reinforced pavement;
(2) Evaluate the benefits of using geosynthetics to reinforce the surface, base layer and/or stabilize weak subgrade soil in a flexible pavement application; and
(3) Suggest the design parameters for geosynthetic-reinforced pavement based on the testing results.

This research will be used to develop, investigate, and refine the understanding of underlying the mechanical behavior and performance of the geosynthetic-reinforced pavement system. The mechanical performance of a geosynthetic-reinforced pavement system will be evaluated in a controlled condition from the LSTW test installed with various sensors such as LVDTs and pressure cells. A numerical simulation will be conducted for a full-scale roadway pavement reinforced with geosynthetics at the different layers. Based on the testing and numerical modeling results, resilient modulus results of reinforced and unreinforced pavement will be obtained to effectively compare the performance between reinforced and unreinforced pavement. This project is directly related to focus areas of the Mid-America Transportation Center in enhancing the safety of road conditions and reducing the negative effects of crashes. The Nebraska Department of Transportation (NDOT) fully supports this project.

Chapter 2 Literature Review

2.1 Proven Geosynthetic Improvement

2.1.1 General

Ground improvement holds significance and has been widely utilized by numerous companies throughout North America. Various methods employed for this purpose include additives, increased compaction levels, and the incorporation of geosynthetics. These techniques are considered cost-effective alternatives, leading to reduced construction times and simplified foundation designs. Generally, pavement structures come in two categories: flexible and rigid. Yoder and Witczak (1975) define a pavement functional failure as one that cannot carry out its intended function without causing discomfort to drivers. With constant demands from traffic on the road structure systems, stresses in the horizontal and vertical directions often show local settlements and cracking. Geosynthetics act as an extremely low-cost insurance that prevent premature failure (Holtz et al. 1998). Their application has been in practice under asphalt roadways since the 1970's, and beginning in the 1980's, geosynthetics took on the reinforcement role to minimize reflective cracking in asphalt overlays, primarily by reducing stress concentration from overhead pressures (Zornberg 2017). The principal function is allotted to additional tensile resistance which absorbs strain and reduces fatigue; geosynthetics change insufficient bearing capacities. When the geogrid is tensioned, it creates an upward force that resists rutting at the surface level (Mounes et al. 2011). Geosynthetics have a role to reduce soil settlement, improve bearing capacity, and reduce base layer aggregate. In short, they improve the performance of unpaved roads by increasing their lifetime while minimizing the maintenance cost and road thickness.

The design of geosynthetics in soft soils can lead to increased tensile strength, increased resistance to reflective cracking and bottom-up fatigue cracking, and increased shearing resistance, which reduces rutting (Zofka et al. 2017). Geotextiles have been the most popular product, and their most common use is for separation and stabilization (Perkins et al. 2005). On closer examination, polypropylene geotextiles have a low manufacturing cost. This is because polypropylene itself is a reliable, cost-effective raw material (Shukla et al. 2006). However, this product works best in non-critical structures as it tends to lose efficiency as proposed loads increase, thus making it more desirable in low-volume environments. To that end, roughly two-thirds of roads are considered low-volume and do not receive this suitable technological attention (Keller 2016).

2.1.2 Stiffness Improvement

Geotextiles are good for separation as they prevent the base and subgrade layers from mixing, thus keeping stability as well. Geogrids are used for reinforcement. These methods can allow for long-term stress reduction in the surface layer in their own ways. When the aggregate is forced to interlock, it is made to act as one unit and uniformly repulses surface-level loading. In this way, it can maintain a high compressive strength. Soil stabilization helps improve the reactive properties to support structures because reinforced soils often show better performance than traditional soils under dynamic loads. Additionally, the soil below hardly changes volume since the rock is not penetrating from above, thus keeping rigidity and structural stability.

This was proven in a study conducted by Al-Qadi et al. (2011) where geogrid was used to improve pavement performance. The test was constructed over weak subgrade where a unilateral dual tire assembly passed overhead at a low speed. It was shown that, indeed, the reinforced sections saw reduced rutting and delayed surface cracking as well as a reduction in horizontal

movement of granular material. The study stated that for weak subgrades, the geogrid should be placed at the base-subgrade interface, as this would help to reduce vertical deflection. According to Motanelli et al. (1997), geogrid placed between a gravel base and sand subgrade showed an increase in CBR for the subgrade. Adams et al. (2015) conducted a CBR test and determined that triaxial geogrid (the same used in the present study) created a 12-31% increase in penetration resistance for soaked and unsoaked conditions when placed in the aggregate layer. Abu-Farsakh et al. (2012) ran a repeated load triaxial test under optimum moisture content. It was concluded that the addition of geogrid reinforcement in granular base specimens showed fewer permanent deformations compared to unreinforced specimens. It also proved that the higher the tensile modulus of the geogrid, the lower the permanent deformation. A triaxial geogrid did the best in this regard. The test showed, though, that geogrid did not greatly improve the resilient modulus of a granular specimen.

Rahman et al. (2014) conducted repeated load triaxial tests with different types of base materials and biaxial and triaxial geogrids. The resilient modulus proved to be higher for reinforced specimens rather than unreinforced. In fact, recycled concrete aggregate (RCA) with biaxial geogrid increased by 24% while the RCA with triaxial geogrid increased 34%. For the same specimens, permanent deformation decreased by 29% and 36%. Oliver et al. (2016) reviewed geogrid stabilization over weak subgrades, specifically the modulus of unbound layers to control particle movement. The research concluded that under triaxial conditions, the resilient modulus was raised by 10% and the stiffness by 5-20% with the addition of geogrid. The bound aggregate had a much lower axial strain after 20,000 cycles. This concept was then applied in the field where geogrid-reinforced subgrade outperformed the control section.

Geosynthetics do not actually increase the structural reinforcement of the pavement itself, but they have been known to decrease earlier on-set damages to roads. Mechanical stabilization with dense granular soil or aggregate base layers has the ability to strengthen the subgrade. It has been shown that adding a geotextile layer to reinforce the granular soil raises the CBR strength (Zumrawi and Abdalgadir 2019). Geotextiles increase the load carrying capacity of soil while the settlement decreases. Moreover, they allow for filtration and drainage and aid in rapid dissipation of excess subgrade pore pressure. In a report by Ogundare et al. (2018), a non-woven geotextile was used as reinforcement and compared against poor subgrade A-7-5 and A-7-6 soils. After conducting a CBR test, it was determined there was an overall 15-20% value increase when reinforcement was added. Additionally, their application, regardless of depth in the subgrade during testing, increased the strength of the soil. Muhmood et al. (2021) showed that the performance of non-woven geotextiles, placed between soft subgrade and the base layer, improved the CBR value roughly 20%.

2.1.3 Rutting Improvement

Geosynthetic reinforcement can lead to rut depth reduction since it leads to an increase in bulk stress, aggregate layer confinement and stiffness, and decreases the vertical stress on the top of the subgrade. Explained by Nunn (1998), rutting could be the result of continuous traffic over too soft of a surface pavement or because of a greater problem beneath the surface. Addition of geosynthetic reinforcement is imperative for roadways to prevent rutting, specifically a small live load (rutting 2-4 inches) or a large live load (rutting greater than 4 inches) on a thin roadway (Holtz et al., 1998). If the actual problem resides in the subgrade, it is determined to be a structural deformation.

For example, many rural roads in India are of poor quality, but are obligated to withstand heavy loads. Without an asphalt cover, the granular base is forced to take the entire load. Latha and Nair (2014) ran both a field and lab test to compare different geosynthetics against load capacity and rut depth. The geosynthetics were placed at the base-subgrade interface. Looking at the final model result, the unreinforced section handled the least amount of pressure while still showing the greatest amount of settlement. The geogrids showed greater pressure resistance. Giroud and Han (2004) suggested an improvement factor for geogrid reinforced unpaved roads. From the field results, it was seen that only planar geosynthetics at higher pressures make a considerable difference, while those at lower pressures are ineffective due to the lack of tensile strain. Barksdale et al. (1989) confirmed this theory and stated that when the aggregate was put under pre-rutting stress, there was greater rut resistance. However, this process is expensive, and so a stiff geogrid was offered as a viable substitute.

Imjai et al. (2019) conducted a series of full-scale field tests to determine the performance of geosynthetics as reinforcement for flexible pavements. The geosynthetic was embedded at different depths, but geosynthetics placed underneath the base layer had the greatest improvement and least amount of rutting. Results showed that vertical static and dynamic stresses were reduced more than 50% in some instances. It also effectively reduced lateral spreading of the aggregate, having the highest lateral strain at only 0.13%. In a static plate loading test conducted by El-Maaty (2016), a woven geotextile and a polyethylene geogrid were compared against a changing base layer thickness to determine a favorable outcome. The test also ran a 0.2 square inch area geogrid, but it should not be considered because it was only used in one case. It was conducted with 0.75-inch nominal aggregate, 0.75-foot thick silty soil subgrade, and the geosynthetic was placed at the soil-aggregate interface. In the end, the higher

area geogrid was the best because it could hold the aggregate in a tighter manner. It showed the greatest contribution when the base layer was the same depth as the subgrade layer. All three geosynthetics showed better resistance to deformation over the unreinforced section.

Appea (1997) used a geotextile, a geogrid, and a control section beneath a granular base to prevent the base and subgrade from mixing. Three different base course thicknesses were constructed (4, 6, and 8 inch), giving nine total test sections, each over a weak clay subgrade. The test lasted over 30 months, and in the end, both geosynthetics performed better than the control section, reducing rutting by nearly 40%. Rutting was the greatest in the 4-inch base course layer, while the other base layers showed relatively the same rutting. Hoppe et al. (2019), in conjunction with the Virginia Department of Transportation, conducted a similar test with the same aggregate base thickness and geosynthetic layout. Using a Falling Weight Deflectometer (FWD), results showed the geotextile sections had lower average deflections, while the geogrid sections proved inconclusive. A belief is because of subtle subgrade differences.

Tingle and Jersey (2005) also performed a test in weak soil and indicated that the control section had the greatest amount of deformation while the use of a geotextile provided the lowest permanent deformation. In both tests, geogrids were in the middle of the pack. The study also concluded the increase in base layer strength was due to cementation during curing. Kermani et al. (2018) wanted to use geotextile as a separator to eliminate unwanted subgrade pumping into the base layer. The study reported an approximate 30% reduction in pavement rutting when geosynthetic was used at the base-subgrade interface. Pumping also decreased. Kazmee et al. (2015) conducted a test where they had several different types of recycled materials to act as a base layer. A mechanical tire drove in a unilateral direction across the strip. It was determined that the three different aggregate types showed virtually little difference from one another, all

with poor rutting improvement. One conclusion drawn from this paper is that it is not as cost-effective nor productive to use recycled aggregates; a geosynthetic could withstand many more cycles before failure was declared.

Fannin and Sigurdsson (1996) conducted a field test with geotextile and geogrid on five reinforced and unreinforced sections of unpaved road. The reinforced sections showed significant improvement. The improvement was the greatest for the thinner layers of base course (1 inch). Leng and Gabr (2002) saw that higher modulus geogrid provided the best reduction in plastic surface deformation. Tensar (2017) ran an in-house test and proved that their triaxial geogrid could reduce surface rutting and permanent deformation by 60% and 35% after 800,000 passes. It showed that aperture size affects the performance for certain aggregate nominal sizes. Sharbaf (2016) determined that rutting was best reduced when either the biaxial or triaxial geogrid was placed in the middle of base layer and not at the bottom of the base.

In the research, Wasage et al. (2004) fabricated a small lab wheel tracking test to measure the rutting resistance of geosynthetic-reinforced low-volume pavement by analyzing the surface rut depth and base deformation. They utilized asphalt, 12-inch thick base and subgrade layers, and six test specimens consisting of two non-woven geotextiles, two biaxial geogrids, and two control sections. The geotextile was placed between the base-subgrade interface layer while the geogrid was placed at the surface-base interface layer. The test concluded at either 10,000 wheel passes or the rut depth became greater than 2 inches. The surface profiles had rut depths which were recorded in accordance with ASTM E1703E 1703M – 95. It was seen that the control sections did not reach 10,000 passes, instead reaching 2 inches at about 8,000 passes. The geotextile had only ¾-inch rutting depth. However, the geogrid specimen showed the greatest rut resistance with less than ½-inch rutting depth. The most evident problem with this research,

though, is the inconsistent placement of the geosynthetics. This kills the comparison. It is believed that if the geogrid were placed under the base layer, it would supply better support, separation, and dissipation from the load.

2.1.4 Case Studies

Barksdale et al. (1989) conducted a large-scale moving wheel laboratory test. A 1,500 force-pound load was applied over an asphalt surface layer that was 1-1.5 inches thick with an aggregate base of 6-8 inches thick. A silty clay was used as subgrade having a CBR of 2.5%. It was decided that reinforcement on soft subgrades should be at the bottom of the base layer. Further, weak subgrades (CBR $\leq$ 3) benefit the most and could lead to a 20-40% reduction in rutting as well as a 10-20% reduction in base thickness. Miuara et al. (1990) reaffirmed the fact that geogrid should be placed at the bottom of the base layer when using poor subgrades (3 < CBR $\leq$ 6) to experience greater rutting resistance. Webster (1993) found that stiffer geogrids work best under the aggregate layer and atop weak subgrades, and they could reduce the total pavement thickness (surface and base layers) by up to 40%. Holtz et al. (1998) as well as Carmichael and Marienfeld (1999) both concluded that the addition of geosynthetics can increase the life of surface roadways by a few years and decrease its thickness need by nearly two inches.

Cuelho and Perkins (2009) performed a field investigation of 10 different geosynthetics on top of a weak sandy clay soil used for subgrade stabilization in conjunction with the Montana Department of Transportation. Longitudinal rutting was monitored. A dual-tandem truck was driven over the test strip until rutting failure occurred, pre-decided at 4 inches. For all cases, the subgrade underperformed before the expected cycles were reached, as only 88 out of 1,000 passes were conducted. It proved that stiffer geogrids provided the best performance and stabilization as opposed to geotextiles and the control section, presumably due to a higher tensile

resistance. Additionally, Chen et al. (2019) determined through numerical pullout analysis that the higher stiffness of a geogrid led to greater active zones with sand particles, which increased resistance. Since geogrid reinforcement is mobilized by the interaction between geosynthetics and soil, it proves that geogrid stiffness plays a foremost role in reinforcement application. Abdi and Arjomand (2011) showed that geogrid resistance is greater in sand than in clay, even if the sand is only a thin layer.

Sun (2015) utilized a large geotechnical test box to find the effect of geogrid-stabilized base over weak subgrade. Cyclic loads were applied at different intervals to see the correlation between the geogrid-subgrade interface. The study used a Dynamic Cone Penetrometer (DCP) to find the CBR value of the subgrade. The equation used was introduced by Webster et al. in 1992. DCP measurements were taken at four different locations along the surface and then averaged for the base course and subgrade after every test. The test concluded that the vertical stresses were reduced with geogrid inclusion or with the increase of a thicker base course. Higher reductions in permanent deformations were also seen. However, the resilient deformations of the geogrid-reinforced sections were larger than the unreinforced sections. It is believed to be due to a bearing failure.

2.1.5 Design Apparatuses

Bagshaw et al. (2015) performed a laboratory wheel tracking test in a 5.5 foot × 5.5 foot × 1.0 foot dimension box. The aggregate was set to the desired moisture and compacted to roughly 95%. A 4,500 force-pound (20 kN) tire load was applied and run in a unilateral direction at a constant speed of around 1 mph. A measurement was taken after every 500 passes. The study measured rutting and deformation of the surface layer. Tests showed that improvement was made with the addition of a geogrid at the base–sub-base interface, cutting the rut depth in half.

The test compared large aperture triaxial geogrid and smaller aperture biaxial geogrid. The results showed that biaxial outperformed triaxial. It is presumed that the aggregate size was better suited for the biaxial geogrid with its appropriate aperture size.

Chapter 3 Materials and Methods

3.1 Materials

3.1.1 Soil Type - Sand

The soil sample selected for this study was sand obtained from a site south of the Platte River and Highway 50 (**Figure 3.1**). Preliminary tests were conducted to find the soil characteristics and were performed following ASTM guidelines. Results from the soil characterization can be seen in **Table 3.1**. **Figure 3.2** shows the grain size distribution of the collected sand. The sand contained hardly any gravel, being mostly medium grained and graded somewhere between poor to well with few fines. All soils were classified using the Unified Soil Classification System (USCS) and ASTM D2487.

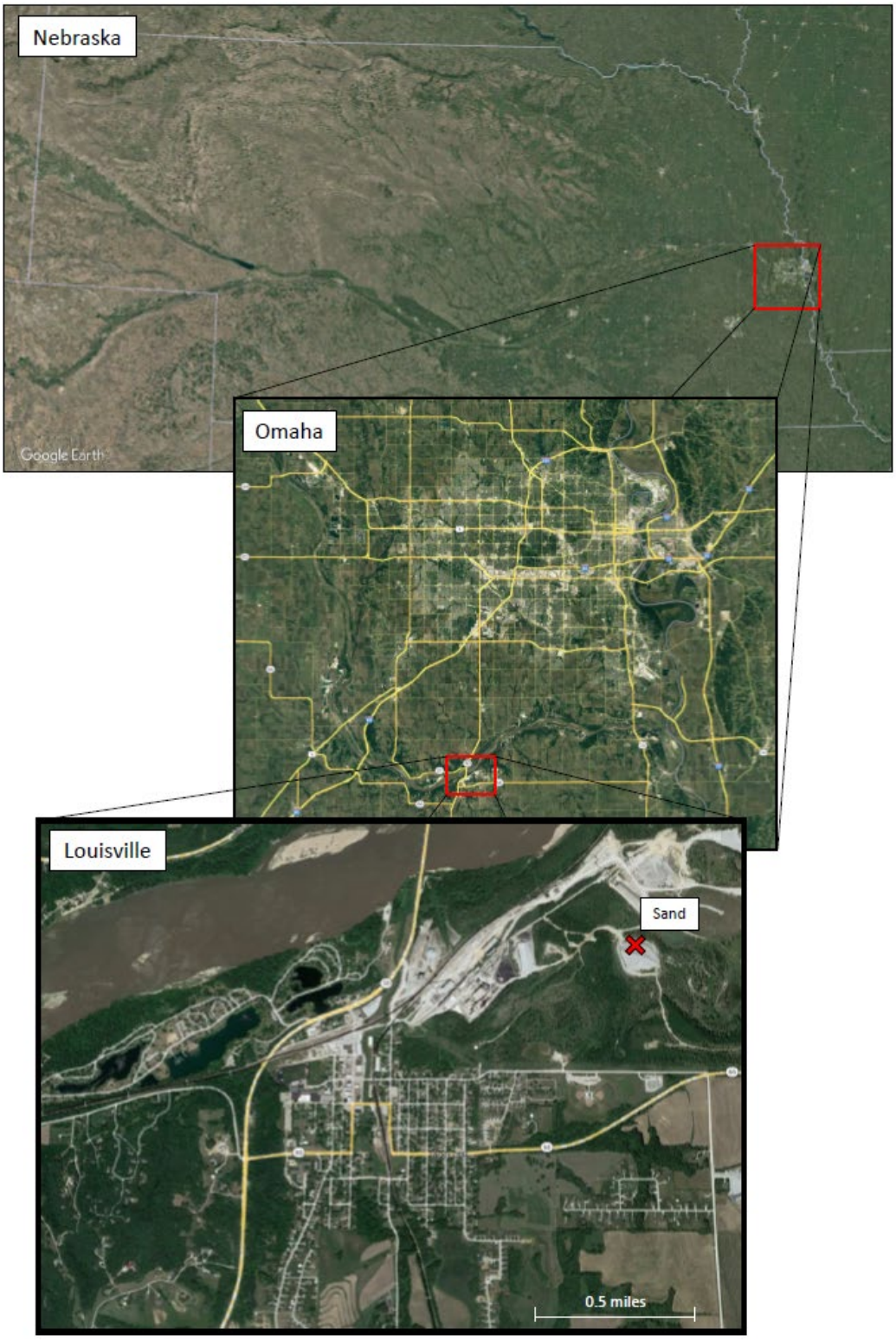

Figure 3.1 Location of sand collection area.

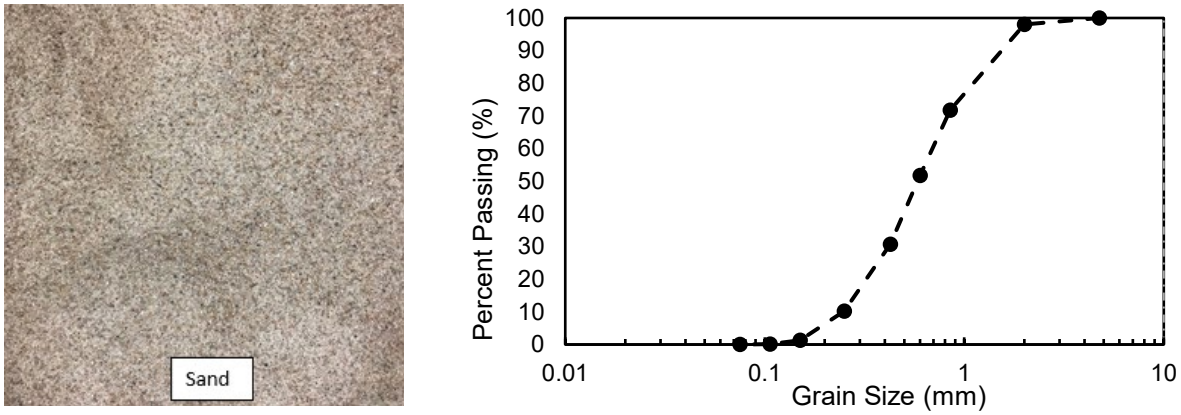

Figure 3.2 (a) Sand Subgrade (b) Grain size distribution graph for sand

Table 3.1 Properties of the sand.

Property	**Value**
D_{60}	0.69
D_{30}	0.41
D_{10}	0.22
Uniformity Coefficient (C_u)	3.14
Coefficient of Curvature (C_c)	1.11
AASHTO Classification	A-1-b
Specific Gravity (G_s)	2.65

3.1.2 Aggregate Characteristics

The aggregate was a well-graded crushed limestone. It was a 1-inch nominal size gradation. **Figure 3.3** shows the distribution for the aggregates used for the Large-Scale Tracking Wheel Test.

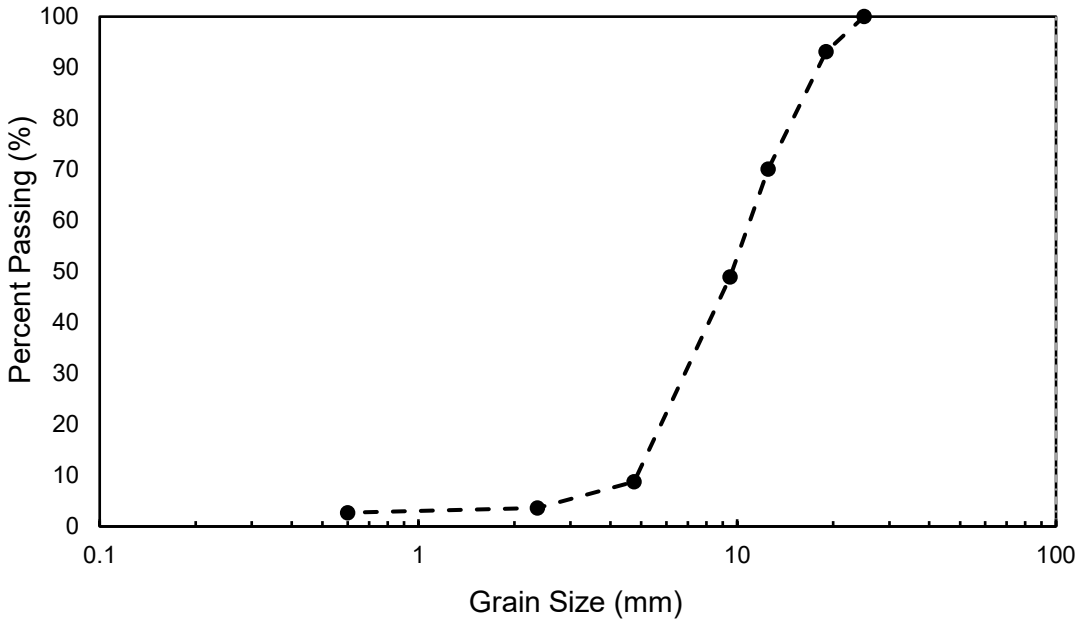

Figure 3.3 Grain size distribution graph for aggregate.

3.1.3 Geosynthetic Type

A biaxial geogrid was the selected geosynthetic for the Large-Scale tracking wheel test due to its high performance in large-scale direct shear test and pullout test which were initially performed for a different project. Tensar International Corporation donated the biaxial geogrid used for this test. The Tensar BX1200 was highlighted for its significance as an initially patented geogrid, a design later emulated by various other companies. This geogrid type is widely used among department of transportation (DOT) agencies around the United States as it adheres standards and specifications set forth by the Federal Highway Administration (FHWA) and the American Association of State Highway and Transportation Officials (AASHTO).

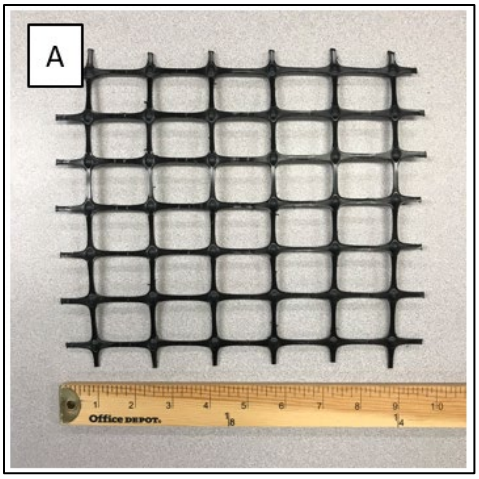

F**igure 3.4** Geosynthetics used for testing, including A) BX1200 (GG1) geogrid

3.1.3.1 Geogrid Characteristics

The GG1 biaxial geogrids are integrally formed from polypropylene materials. The biaxial geogrid has square-shaped apertures with intersection points that are known as junctions. The ribs are the stretched strands that complete the shape at said intersections. and **Table 3.2** show the characteristics of these geogrids.

Table 3.2 GG1 geogrid characteristics.

Structural Integrity		
	MD[1]	XMD[2]
Aperture Dimension, in	1.0	1.3
Minimum Rib Thickness, in	0.05	0.05
Tensile Strength at 2% Strain, lbs/ft	34.2	620.0
Tensile Strength at 5% Strain, lbs/ft	67.5	1340.0
Ultimate Tensile Strength, lbs/ft	109.2	1970.0
Index Properties		
Junction Efficiency, %	93.0	
Flexural Stiffness, ft-lbs	0.054	
Aperture Stability, N-m/deg	0.650	

[1] Machine Direction
[2] Cross-Machine Direction

3.2 Methodology

3.2.1 Apparatus Set-up

The research team at the University of Nebraska-Lincoln designed and constructed the Large-Scale Tracking Wheel (LSTW) testing apparatus specifically for this project. The mechanical performance of geosynthetic-reinforced pavement layers was evaluated. The test conditions closely mirror real-world field conditions, particularly in aspects of dimensions and the frequency of cyclic loadings. To assess the long-term rutting performance of the pavement, the team performed cyclic loading tests on the pavement layer, monitoring the progression of rutting over time. Additionally, the impact of geosynthetics on the strength of pavement layers, as well as the changes in pressure at the interface between the subgrade and basecourse was evaluated.

The design of the box was taken in part from research performed by Bagshaw et al. (2015) and Kim et al. (2018) in conjunction with the Georgia Department of Transportation. The test was conducted for soil-geosynthetic interaction under a base layer. The box was one steel piece with additional ribs on the sides to help provide reactionary stiffness. The interior of the box was spray-painted with a black gloss to minimize friction and to prevent rust. The large-scale box was constructed with 5.5-foot wide, 5.5-foot long, and 2.0-foot tall (1.67 meter × 1.67 meter × 0.61 meter) internal dimensions. The layout and full assembly is shown in the **Appendix**. The box was placed atop a track that was doweled into the floor. The track was made from c-channel steel with four outer plate extensions with holes in them for the dowels to pass through. These extensions were bolted to the inner track at one end and doweled into place on the other to stabilize the track. The box was attached to a pulley frame which was in turn connected to a motor and the crank arm to push and pull the box in a unidirectional motion. Ten wheels were attached to the bottom of the box to aid with unidirectional movement. These wheels were greased to reduce the heat generated from friction during testing. The tire used during testing to apply cyclic loading on the base coarse surface had a 30-inch diameter with a 7.5-inch width to hold a maximum load of 3000 lbs (1360 kg) at 80 psi (550 kPa) tire pressure. A mounted ball bearing with two-bolt flange was placed in the wheel and connected to the setup frame by a 6-foot high-strength carbon steel rod. This enabled the tire to rotate freely in place. A hydraulic actuator was used to apply a load of approximately 10kN through the rectangular steel frame onto the wheel road. The test was run at an approximate speed of 1 mph (0.447 m/s). The complete set-up is shown in **Figure 3.6**.

Figure 3.5 Tire used for LSTW test

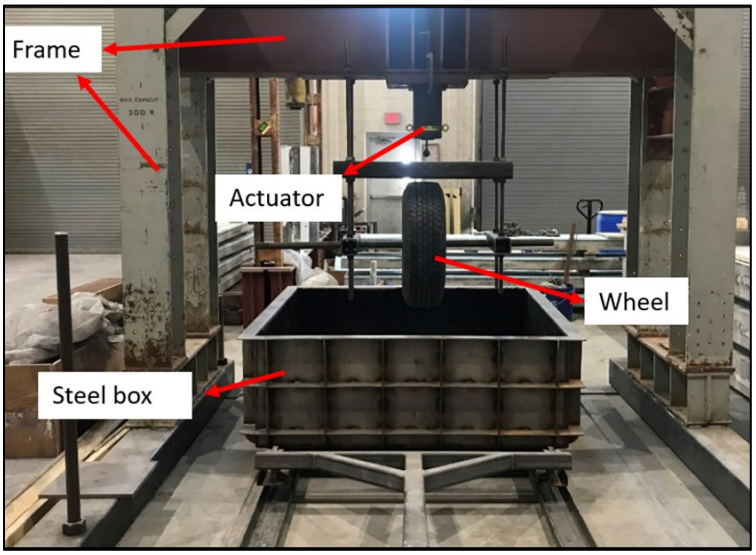

Figure 3.6 Complete set-up of the Large-Scale Tracking Wheel (LSTW) test

3.2.2 Testing Matrix

For the Large-Scale Tracking Wheel Test, three distinct scenarios were examined to determine the extent of reduction in permanent deformation, pressure reduction at layer interface, and the changes in strength/stiffness of the pavement layers due to the use of geosynthetics. Details of these evaluations are presented in **Table 3.3**.

Table 3.3. Large Scale Tracking Wheel (LSTW) testing matrix.

Case	ID	Condition	Base thickness (in.)	Subgrade thickness (in.)
1	Control	No Geosynthetics	12 in	12 in
2	GG1 – 12 in	Geosynthetic reinforced (GG1)	12 in	12 in
3	GG1 – 9in	Geosynthetic reinforced (GG1)	9 in	12 in

3.2.2.1 Case 1 – Control Test Preparation

Sand was selected as the subgrade layer for this test. The sand was first air-dried before used. The steel box was filled with air dried sand and compacted with a heavy-duty plate compactor, as shown in **Figure 3.7**, to a relative density of approximately 80% in two lifts approximately 6 in thick. The compacted sand layer can be seen in **Figure 3.8**. The total thickness of the sand layer was approximately 12 in.

The aggregates used for the base course were prepared at OMC (2.75%) using a concrete mixer (**Figure 3.10**). The base course layer was then placed in two lifts approximately 6 inches thick and compacted with a heavy-duty place compactor to a relative density of approximately 95%. The compacted aggregate base course layer can be seen in **Figure 3.11**.

3.2.2.2 Case 2 – GG1 12 in Test Preparation

In this scenario, a geogrid (GG1) was utilized between the interface of the subgrade and base layers. The arrangement consisted of a sand subgrade layer about 12 inches thick, topped by a 12-inch base layer directly above the geogrid. The compaction process for both the sand and base layers mirrored that of the control case, achieving similar relative densities. To ensure that the geogrid remained flat and extended, steel plates were employed to secure it to the top of the sand subgrade layer, as depicted in **Figure 3.9**.

3.2.2.3 Case 3 – GG1 9 in Test Preparation

In this case, a geogrid (GG1) was placed between the subgrade and base layers. The thickness of the sand subgrade layer was maintained at approximately 12 inches, while the base layer was made thinner to evaluate the performance of a reinforced pavement with a reduced base layer. Steel plates were utilized to securely attach the geogrid to the top of the sand subgrade layer, ensuring it remained flat and properly stretched. For compaction, both the sand and aggregate layers were compacted in two sublayers to relative densities of approximately 80% and 95%, respectively.

Figure 3.7 Heavy duty plate compactor.

Figure 3.8 Compacted sand subgrade layer.

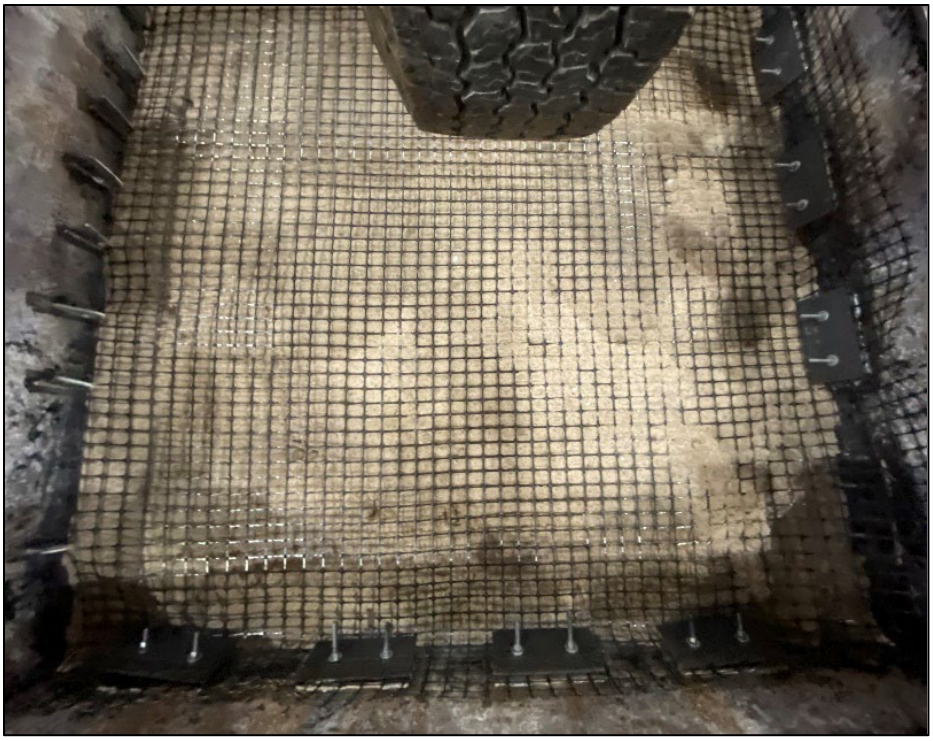

Figure 3.9 Installed geogrid on sand subgrade.

Figure 3.10 Aggregate mixing at OMC using concrete mixer.

Figure 3.11 Compacted aggregate base course layer.

3.2.3 Large Scale Tracking Wheel Test Instrumentation

3.2.3.1 Linear Variable Displacement Transducer

Six LVDTs from Harold G. Schaevits Industries with a measuring range of 2 in were used to record the vertical deformation of the base layer. These were made from industrial duty material for resistance to dust, temperature, shock, and variability. The vertical deformation recorded showed how rutting progressed during the test. These were fixed along a wooden beam that was held in place by a threaded rod on the sides of the steel box with bolts at the top and bottom to prevent movement during testing. The LVDTs were installed at the center of the steel box at equal intervals approximately six inches along the wooden beam as shown in **Figure 3.12**. All LVDTs were calibrated before usage. The coefficient of determination (R^2) for LVDTs, representing the linear relationship between the voltage and calibrated readings, ranges from 0.9979 to 1.0, as highlighted in **Table 3.4**. This range signifies the accuracy and precision of the

LVDTs readings. The LVDTs were connected to a Keysight DAQ970A 20-channel data logger using the Benchvue software.

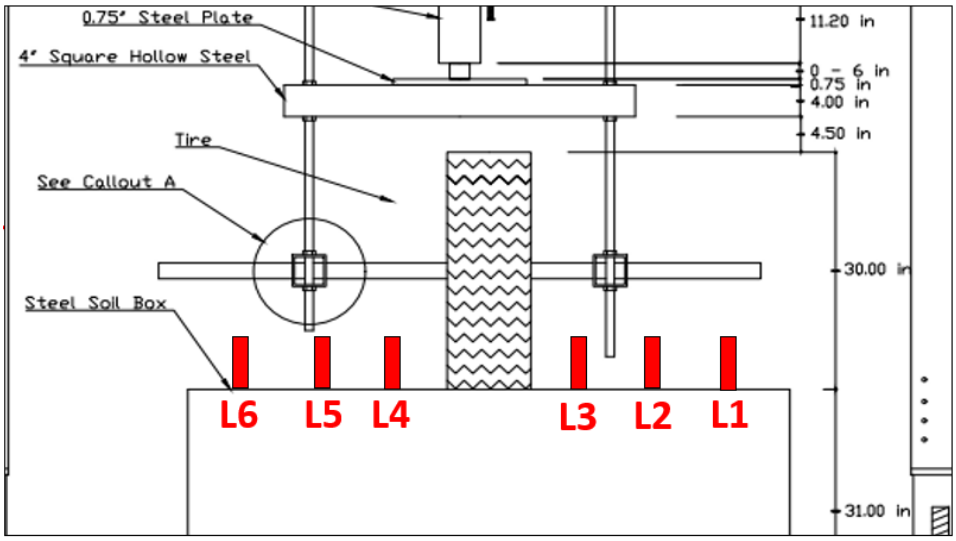

Figure 3.12 LVDT positions in steel box

Table 3.4 LVDT R^2 summary

LDVT	R^2
1	0.9996
2	0.9996
3	0.9996
4	0.9979
5	0.9982
6	1.0

3.2.3.2 Pressure Cells

Three pressure cells were used for this test. They were stainless steel with excellent corrosion resistance from Tokyo Measure Instrument Lab. They have a 50 mm outer diameter and a dual diaphragm structure (**Figure 3.13**). The pressure cells were calibrated by applying

different loads with the help of a calibrated actuator. A linear trend was established from which an equation was obtained for the relationship between the pressure and output voltage. The R^2 for the three pressure cells used are found in **Table 3.5**. The pressure sensors were also connected to a Keysight DAQ970A 20-channel data logger using the Benchvue software. Two pressure cells were installed on top of the compacted subgrade layer for Case 1 (**Figure 3.14**) and a third pressure cell installed on the top of the compacted base course layer (**Figure 3.16**). For Case 2 and 3, one pressure cell was installed beneath the geosynthetic at the base and subgrade interface and a second pressure cell installed on top of the geosynthetic, as shown in **Figure 3.17**. The third pressure cell was installed on top of the base layer in a similar manner was the Control test. These pressure cells were used to monitor pressure exerted on top of the base layer and at the subgrade and base interface and during testing. The schematic of the individual pressure cell positions can be seen in **Figure 3.17**.

Table 3.5 Pressure Cell R^2 Summary.

Pressure Cell	**R^2**
1	0.9999
2	0.9996
3	0.9990

Figure 3.13 TML Pressure cells

Figure 3.14 Pressure cell on compacted sand layer.

Figure 3.15 Pressure cell installed on top of geosynthetic location.

Figure 3.16 Pressure cell installed on top of base course.

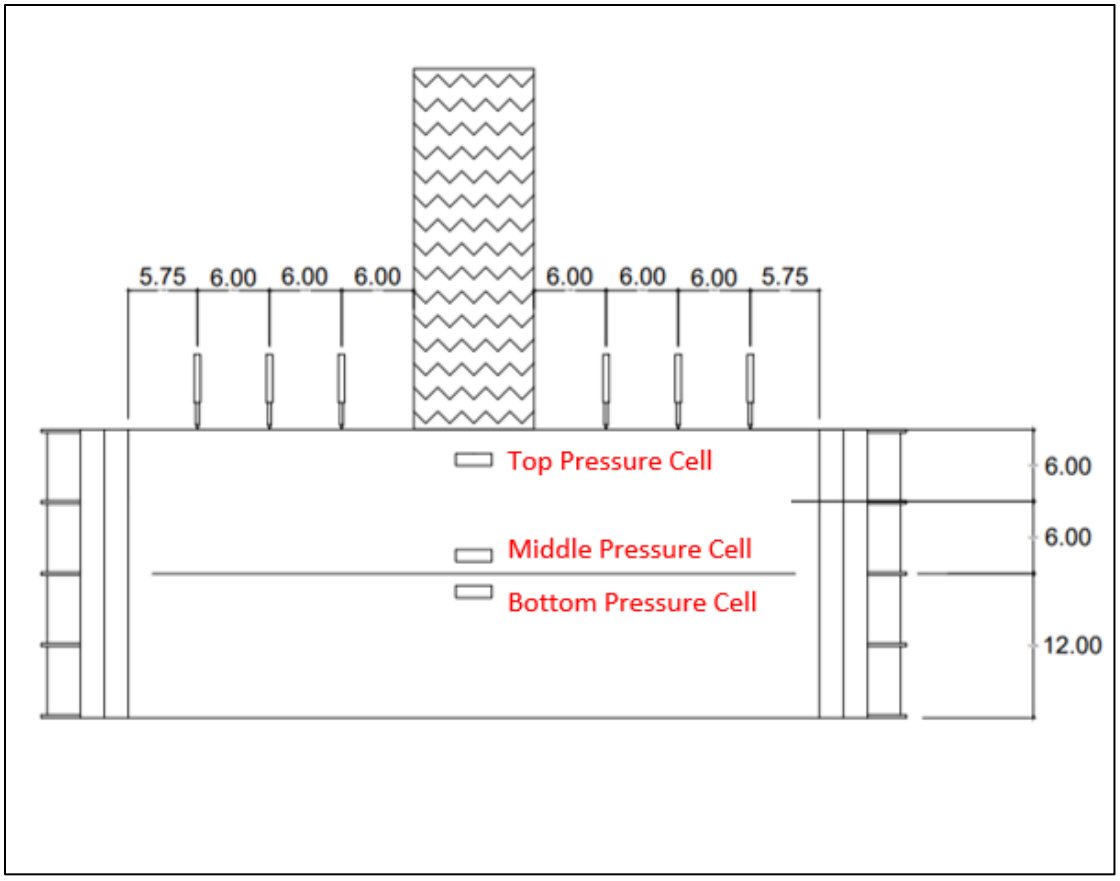

Figure 3.17 Schematic of pressure cell positions (unit, inches).

3.2.3.3 Load Cell

A load cell was installed beneath the hydraulic piston to measure the load that would be applied during the test as shown in **Figure 3.18** and **Figure 3.19**. Assisted by an electric hydraulic pump system, an approximate load of 10 kN was applied through the actuator. The applied load was continuously monitored using a load cell and adjusted throughout testing.

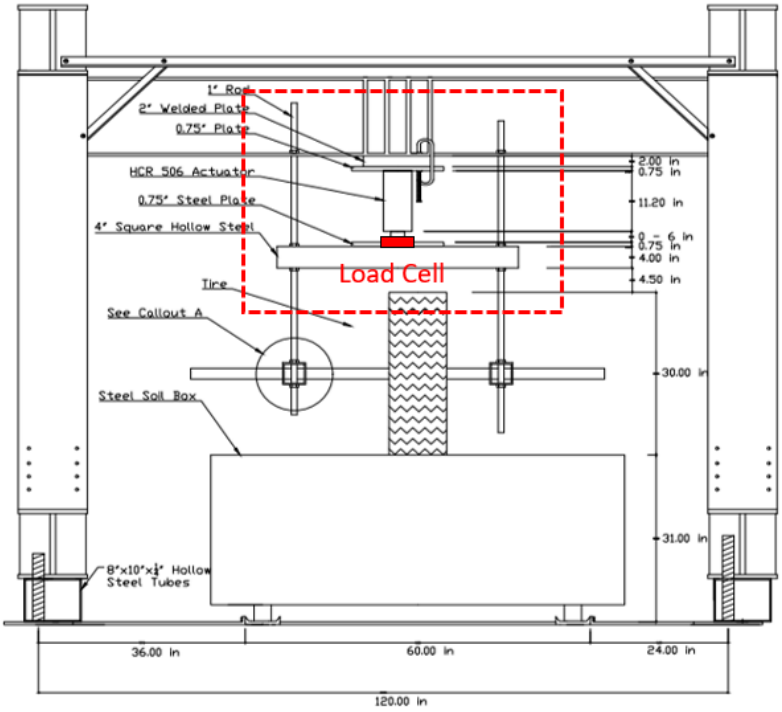

Figure 3.18 Schematic of load cell position (unit, inches).

Figure 3.19 Load cell positioned beneath actuator.

3.2.4 Test Run

The load cell, linear vertical displacement transducers (LVDTs) and pressure cells were connected to their respective power supply units and data acquisition box. The data acquisition box was then connected to a laptop to record the data during testing. The wheel was gently lowered onto the surface of the steel box. The test setup was then turned on from the control unit. The unidirectional motion was initiated with the test run at a speed of approximately 1 mph. The complete testing setup in shown in **Figure 3.20**. Results for each case are discussed further in **Section 4.1**

Figure 3.20 LSTW complete test setup.

3.2.5 Dynamic Cone Penetrometer (DCP) Test

The Dynamic Cone Penetration Test provides a measure of a material's in-situ resistance to penetration. Schematic of the DCP device is shown in **Figure 3.21**. The number of blows required for the cone to penetrate a specific depth (usually measured in mm/blow) gives an indication of the soil's strength and is called Dynamic Penetration Index (DPI). This test was conducted before and after applying rolling wheel loads to the surface of the prepared pavement layers. The DPI was correlated with the resilient modulus to provide an indication of how the stiffness/strength within the pavement layer changes for both geosynthetic reinforced and unreinforced cases.

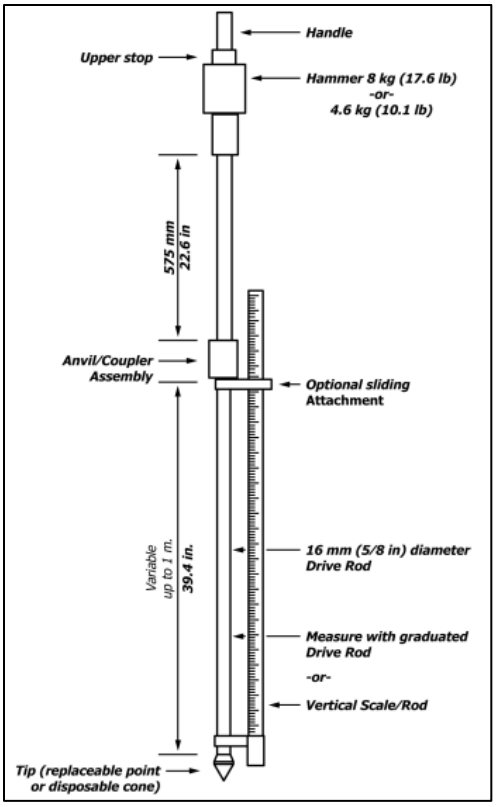

Figure 3.21 Schematic of DCP device

3.2.6 FLAC Model

The term FLAC stands for "Fast Lagrangian Analysis of Continua" and it is a numerical modeling software for advanced geotechnical analysis of soil, rock, and groundwater in a two-dimensional plane. It utilizes an explicit finite difference formulation that can model complex behaviors, such as problems that consist of several stages, large displacements, or even non-linear material behavior. Materials are represented by zones, known as elements, which form a grid, or a mesh. Each element, in turn, follows a prescribed linear or non-linear stress-strain law in response to the applied force and boundary restraints. Often, a higher force will cause the meshed diagram to deform and shows the applicable movement of the deformation (FLAC 2022).

Structures such as tunnels, sheet piles, or roads can be modeled. In this regard, it is possible to examine the effects of instability with concrete, steel, or soils. The simulation investigation tried to find the surface settlement of different soil types against different geosynthetics, similar to the research properties in the present study. The interlocking and junction effect of the soil-reinforcement was considered by adapting a composite stiffness that was comprised of the soil and geosynthetic in the simulation (Eun et al. 2017). The model was validated with existing cases in literature (Kim et al. 2021) as well as the Direct Shear and Pullout tests. **Table 3.6** shows the case literature that filled in the blanks. The cable element in FLAC has been shown to provide a good representation of geosynthetic materials (Holtz and Lee 1998; Vulova and Leshchinsky 2003; Ebrahimian 2011; and Zheng and Fox 2017).

FLAC requires the user to first establish the model type as well as the parameters for the materials that will be used. A Mohr model was used with the given parameters. A grid was created and then the mesh was applied across the grid. The mesh was generated into smaller trapezoidal elements per grid element, that way when the figure deformed, it would show a clearer settlement. A cross-section of the road was developed with the grid, specifically looking at an asymmetrical layout. Hence, smaller grids were generated under the tire load to create a more accurate simulation. The simulation further broke the cross-section into three parts, which became the asphalt roadway, the aggregate base layer, and the subgrade soil. The asphalt was determined to be half a foot in depth while the base layer was a foot deep. The subgrade soil constituted the rest of the layout, and it was 20 feet in depth—more than enough to negate the boundary effect from the bottom.

As it stood in the simulation, the cross-section was “floating” in space, meaning that if a load were applied at this time, the whole grid would shift down together and there would be no

conclusive settlement. The boundaries, therefore, needed to be fixed. The sides of the cross-section were fixed in the horizontal direction, representing roller connections. The simulation was still free to move in the vertical direction. The base of the model was fixed in both the horizontal and vertical directions. The properties of the three layers were applied. These properties were taken largely in part from the direct shear and pullout tests which were performed earlier as part of a different project, as previously mentioned. Once the properties were in place, the geosynthetic was added. The simulation made a biaxial geogrid, a triaxial geogrid, and a geotextile. The properties were representative of the current research. The geosynthetics were placed at a different depth to correspond with the same 13 kPa confining stress. The sand had an assumed density of 1900 kg/m^3, so its depth was 0.70 meters. The 40,000 Newton load was then applied to the cross-section shown in **Figure 3.22**.

Table 3.6 Layer type parameters used in study.

Parameter	Layer Type		
	Asphalt	**Granular Aggregate**	**Louisville Sand**
Modulus of Elasticity (psi)	174,100	4,800	7,300
Density (pcf)	144	133	118
Poisson's Ratio	0.25	0.30	0.25
Cohesion (psi)	0	0	0
Friction Angle (°)	0	65	30
Dilatancy Angle (°)	0	6	0

References: Hatami and Bathurst (2001), Iowa DOT (2015), Lambe and Whitman (1969), NDOT (1990), Radhakrishna and Klym (1974), Rajagopal et al. (2014), Subramanian (2006), Song et al. (2018), Tan et al. (2017), and Zheng et al. (2014).

Table 3.7 Cable element parameters used in study.

Parameter	Sand		
	Biaxial Geogrid	Triaxial Geogrid	Geotextile
Modulus of Elasticity (psi)	150,000	120,000	70,000
Bond Stiffness, kbond (psf)	36,600	33,400	20,000
Bond Strength, sbond (lbf/ft)	560	450	320
Bond Friction Angle, sfriction (°)	35	37	30

References: Abdi and Arjomand (2001), Iowa DOT (2015), and Zheng et al. (2014).

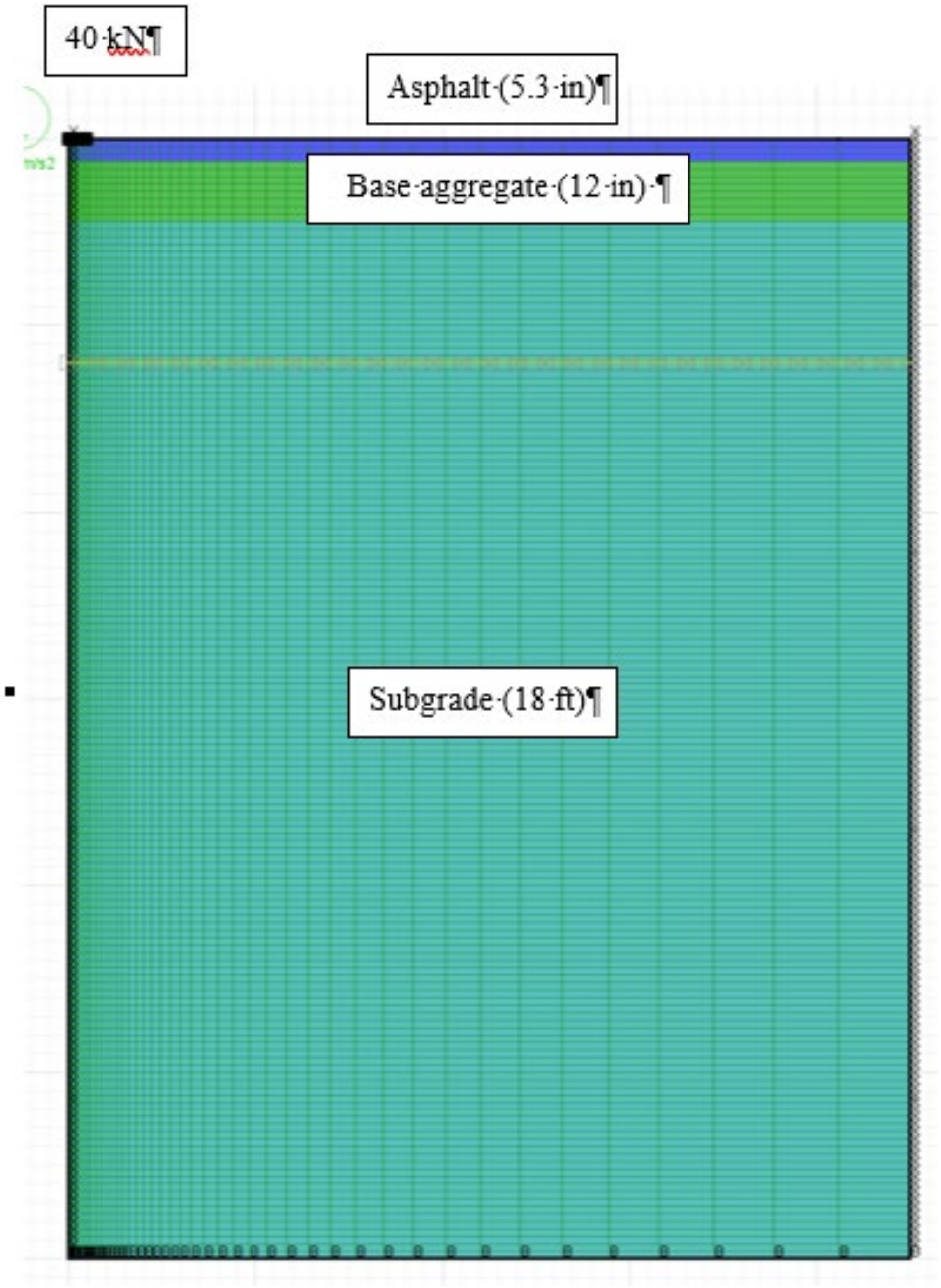

Figure 3.22 Cross-section of the asymmetric roadway with the geosynthetic and load.

Chapter 4 Results and Discussion

4.1 Analysis of LSTW test

Three key parameters were assessed across the three cases to understand the impact of the use of geosynthetics on pavement layers. This included strength/stiffness, as reflected by Dynamic Cone Penetration (DCP) indices, permanent deformation, and the pressure reduction effects.

4.1.1 Evaluation of Pavement Strength/Stiffness

DCP tests were conducted before and after applying the rolling wheel test on the pavement layer of the LSTW test to evaluate the change in strength of the pavement layer. **Figure 4.1** shows the cumulative blows against depth for the three cases. GG1-12 in showed the best performance in terms of increase in strength/stiffness of the entire pavement layer after the rolling wheel load application. GG1-9 in also showed a relatively better performance in terms of increase in base course layer strength compared with the control case.

The profile of DPI with depth for the three cases can be found in **Figure 4.2**. The confining zone above the geogrid due to interlocking effect of the geosynthetic was identified and was more profound in the GG1-12 in A than the GG1-9 in A. GG1-12 in A also showed the highest level of improvement in both the base course and the subgrade strength/stiffness. GG1-9 in A showed an increase in the base course strength/stiff but a reduction in the subgrade strength compared to Control A. This reduction in subgrade strength for GG1-9 in A can be attributed to the reduced confining stress acting on the pavement layer with the reduction in the pavement thickness. The reduction in the base course thickness resulted in a reduction in the subgrade restraint which plays a primary role in improving the subgrade strength. **Figure 4.3** and **Figure**

4.4 shows the percentage reduction in the layer DCP indices for the three base and subgrade layer cases.

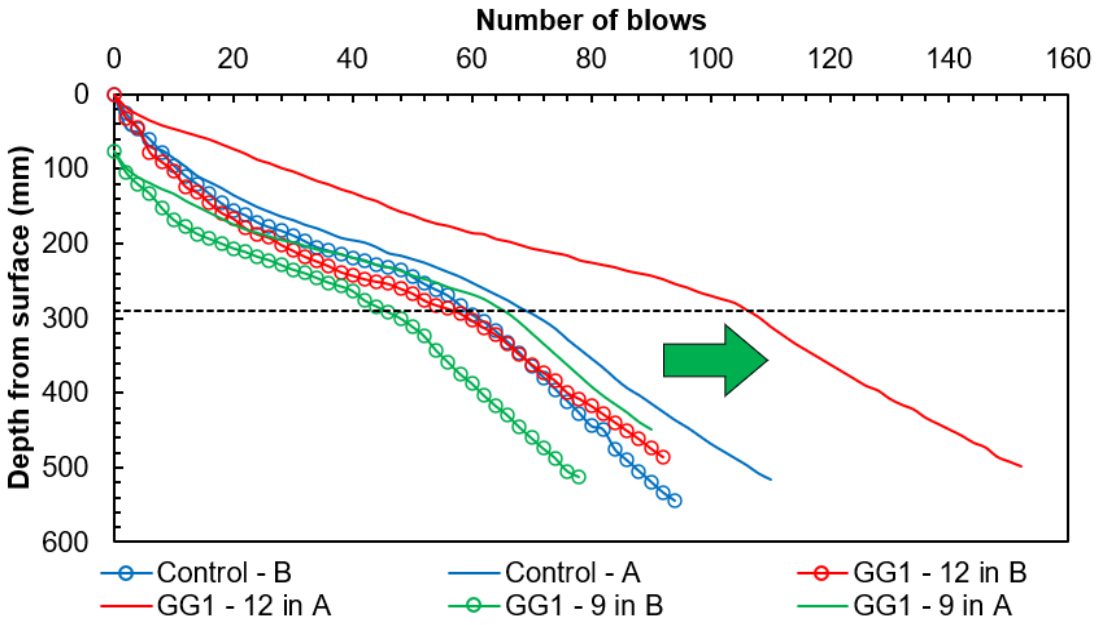

Figure 4.1 Cumulative blows vs Depth

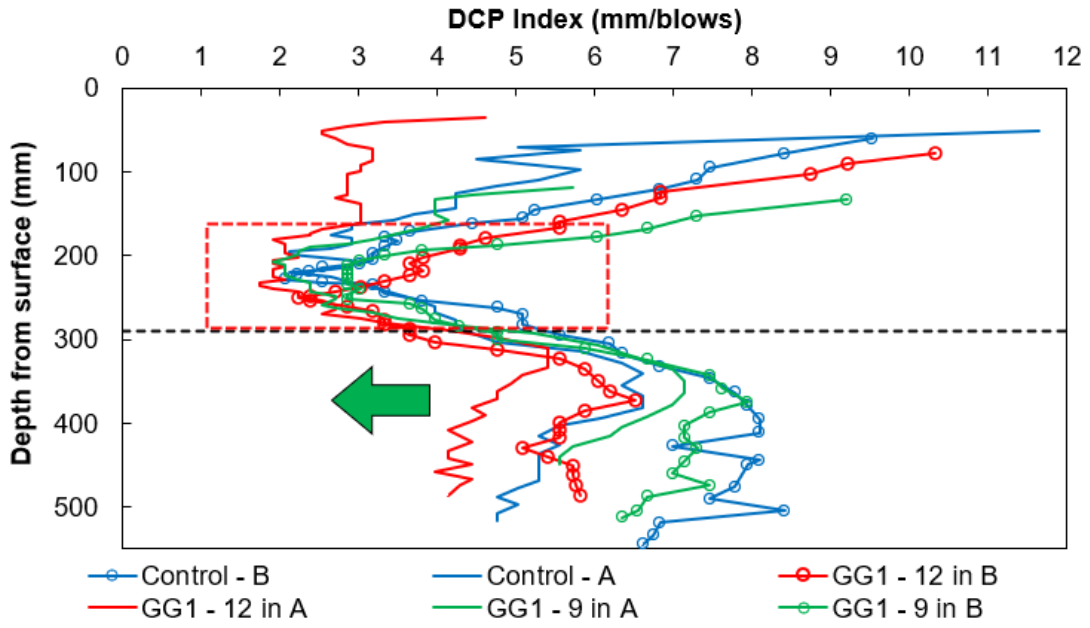

Figure 4.2 DPI vs Depth

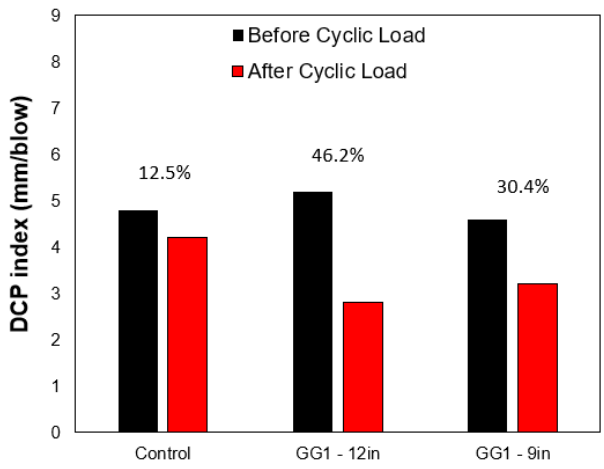

Figure 4.3 Base Course DPI comparison.

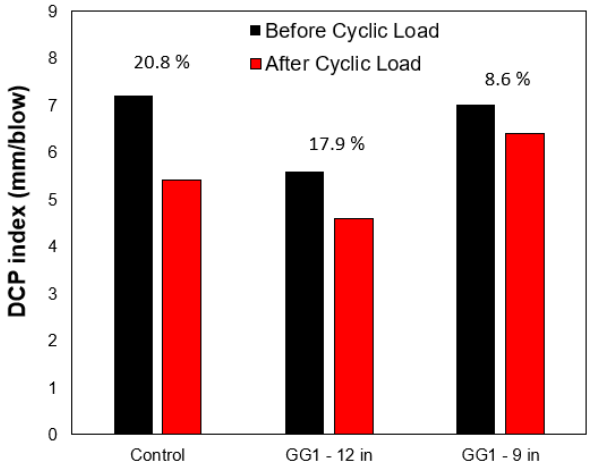

Figure 4.4 Sand subgrade DPI comparison.

4.1.2 Correlation between DPI and other parameters

Using correlation by Lin et. al (2005), Harison (1986) and Mohammad et al. (2008), the Resilient Modulus, CBR and Subgrade modulus of reaction were computed from the DPI for all three cases as shown in **Table 4.1. Figure 4.5** and **Figure 4.6** highlight the increase in resilient

modulus for the three different cases and layers both before and after the rolling wheel loading using the correlation by Lin et al. 2005. Case 2 showed the highest increase in resilient modulus of the base layer after the LSTW test with a 50.8% increase while Case 3 showed a 27.2% increase in the resilient modulus (**Figure 4.5**). For the sand subgrade, Case 2 showed the highest increase in the resilient modulus of 14% followed by the Control with an increase of 21% and a 6% increase in the resilient modulus of Case 3 (**Figure 4.6**).

Table 4.1 Correlations between DPI and strength parameters.

Correlation	**DPI (mm/blow)**		**Mr (psi) (Lin et. al. 2005)**		**CBR (%) (Harison 1986)***		**Ks (MN/m3) (Mohammad et. al. 2008)**	
Case:1	Control							
Layer	B	A	B	A	B	A	B	A
Base course	4.8	4.2	27544	30098	50	58	218.82	246.79
Subgrade	7.2	5.4	21043	25472	32	44.14	151.85	196.79
Case:2	GG1-12 in							
Layer	B	A	B	A	B	A	B	A
Base course	5.2	2.8	26118	39396	46	92	203.59	355.62
Subgrade	5.6	4.6	24864	28334	42	53	190.44	227.37
Case: 3	GG1-9 in							
Layer	B	A	B	A	B	A	B	A
Base course	4.6	3.2	28334	36053	53	79	227.37	315.31
Subgrade	7	6.4	21440	22754	33	37	155.76	168.85

Table 4.2 Resilient modulus evaluation before rolling wheel load application.

Case	**DPI Before**	**Mr (psi)**	**% increase**
Control	7.2	21042.8292	-
GG1-12 in	5.6	24864.2897	33.0
GG1-9 in	7	21440.1495	14.6

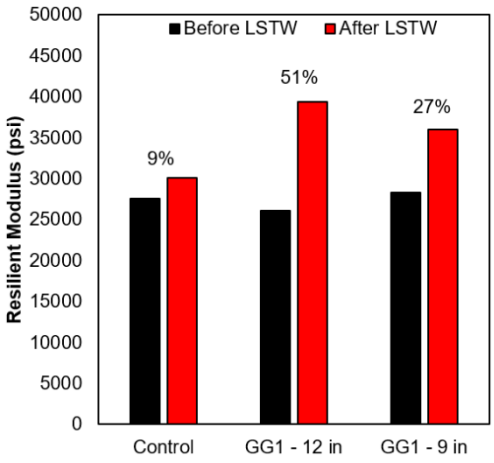

Figure 4.5 Resilient modulus estimate – base.

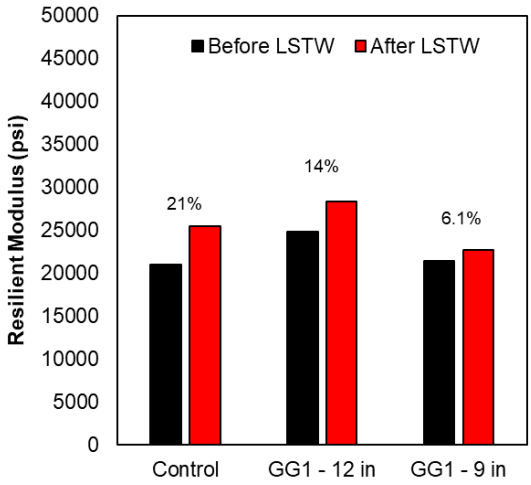

Figure 4.6 Resilient modulus estimate – subgrade.

4.1.3 Evaluation of Permanent Deformation (Rutting)

The total vertical deformation (rutting) that occurred beneath the tire at the top surface of the base course layer was measured after the rolling wheel load was applied for the three cases using a measuring tape. **Figure 4.7** shows the total deformation recorded for the 3 cases. With the use of the geogrid, the total permanent deformation reduced from 44 mm for the Control to 29 mm, which represents a 34.1% reduction for Case 2. Comparing Case 1 which was the control to Case 3 (reduced base coarse thickness), the total permanent deformation reduced from 44 mm to 31 mm, which represents a 29.5% reduction. This highlights the profound impact of geosynthetics in reducing the total permanent deformation of the pavement system.

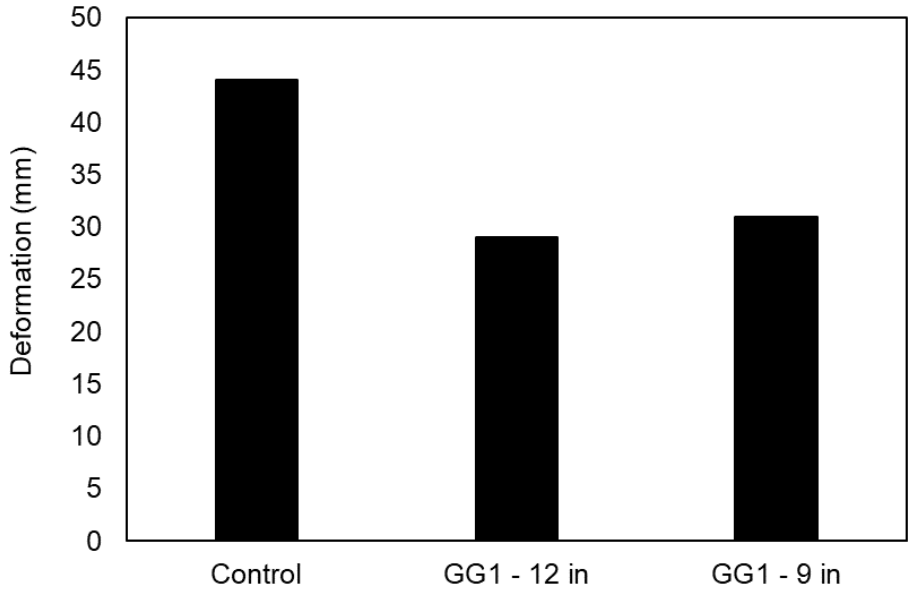

Figure 4.7 Deformation comparison

The six LVDTs installed on the sides of the wheel also recorded the total deformation for Case 1 and Case 2. **Figure 4.9** to **Figure 4.14** show the total deformation recorded by the six LVDTs. Comparing the deformation measured for the Control to Case 2, a significant reduction in the total deformation was observed in the use of geogrid. This can primarily be attributed to the geogrids lateral restraint effect which provided more resistance to deformation and the interlock effect the geogrid provides at the subgrade and base interface increasing the strength of the pavement layers. The deformation reduction with the use of geosynthetic is more prominent in LVDT 3 and LVDT 4, which are the closest to the point of application of the wheel loading. This deformation reduces the position of the LVDT increase from the point of application of the wheel loads.

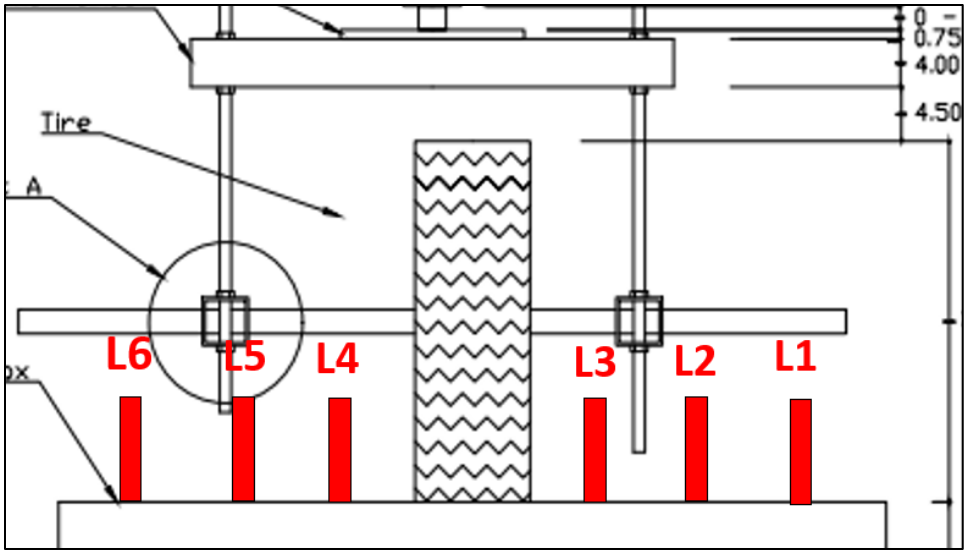

Figure 4.8 LVDT positions in LSTW setup.

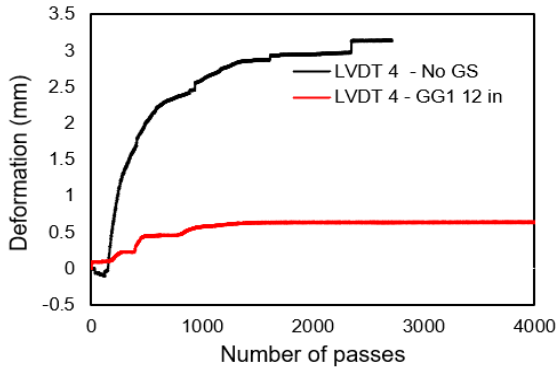

Figure 4.9 LVDT 4 deformation readings.

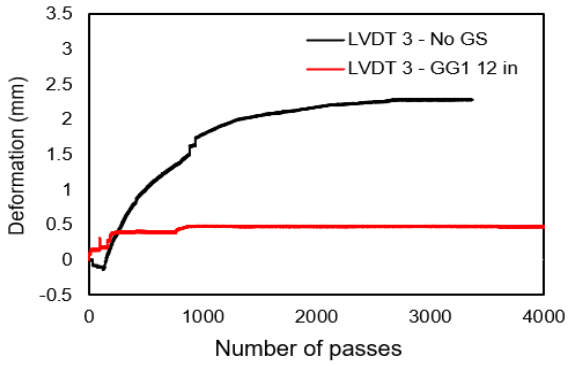

Figure 4.10 LVDT 3 deformation readings.

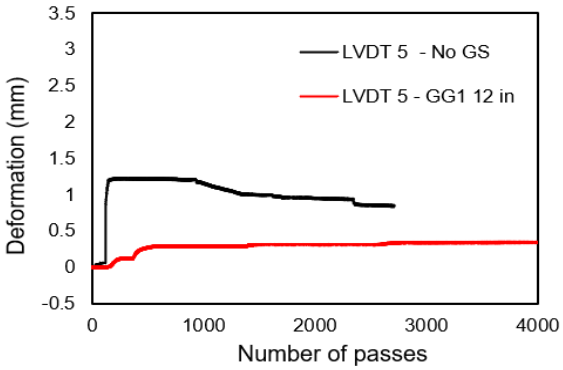

Figure 4.11 LVDT 5 deformation readings

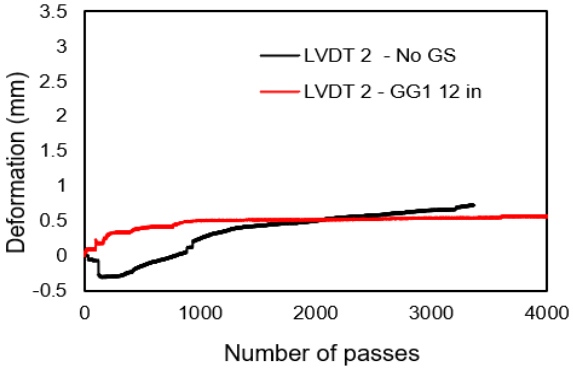

Figure 4.12 LVDT 2 deformation readings.

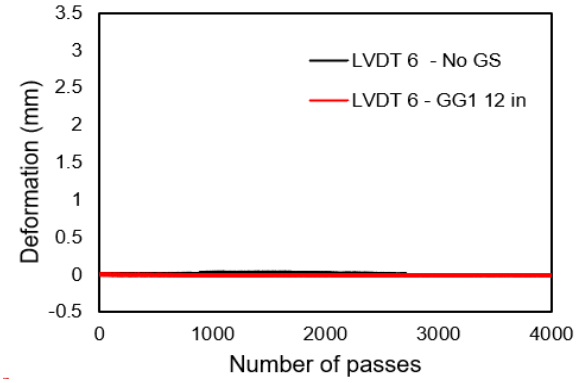

Figure 4.13 LVDT 6 deformation readings.

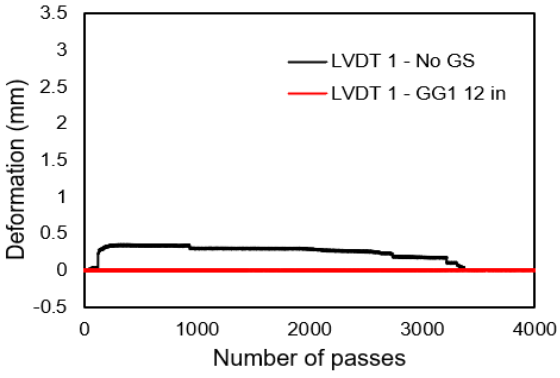

Figure 4.14 LVDT 1 deformation readings.

4.1.4 Pressure Reduction Effect

Figure 4.15 shows the typical rolling wheel loads applied on the pavement surface taken over a 1-minute period. The pressure cell reading recorded by the top, middle, and bottom pressure cells taken over a 1-minute period are shown in **Figure 4.16**, **Figure 4.17**, and **Figure 4.18** respectively.

The pressure distribution within the pavement layer for the three cases were analyzed to show how pressure reduction occurs at the subgrade/base interfaces. **Table 4.3** shows the pressure acting at the base and subgrade interface for the middle and bottom pressure cells. The reduction in pressure from the middle to the bottom pressure cell is highlighted in **Figure 4.19**. The Control test had the least reduction in the pressure between the middle and bottom pressure cell. Difference in pressure cell reading for the middle and bottom pressure cell can be attributed to the position difference between these two pressure cells. The pressure acting on the subgrade/base interface decreased by 13.2% and 19.5% for Case 2 and 3, respectively, which highlights the significant effect geogrid has in pavement, as shown in **Figure 4.20**. This further reduction can be attributed to the geosynthetic as part of the stress acting at the interface of the subgrade and base is transmitted into the geosynthetic.

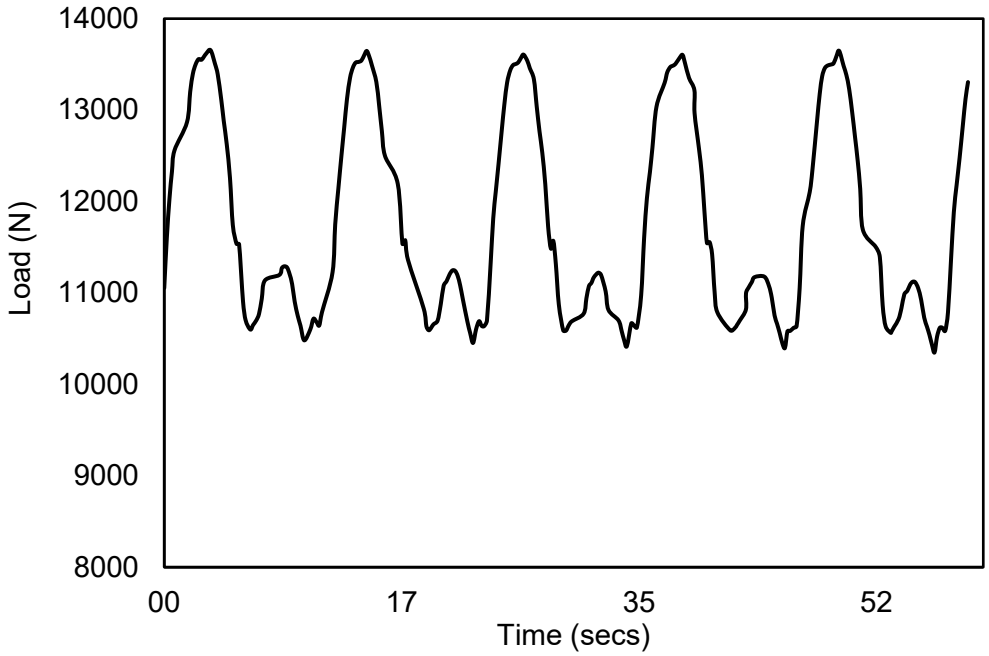

Figure 4.15 Load cell reading taken over 1-minute period.

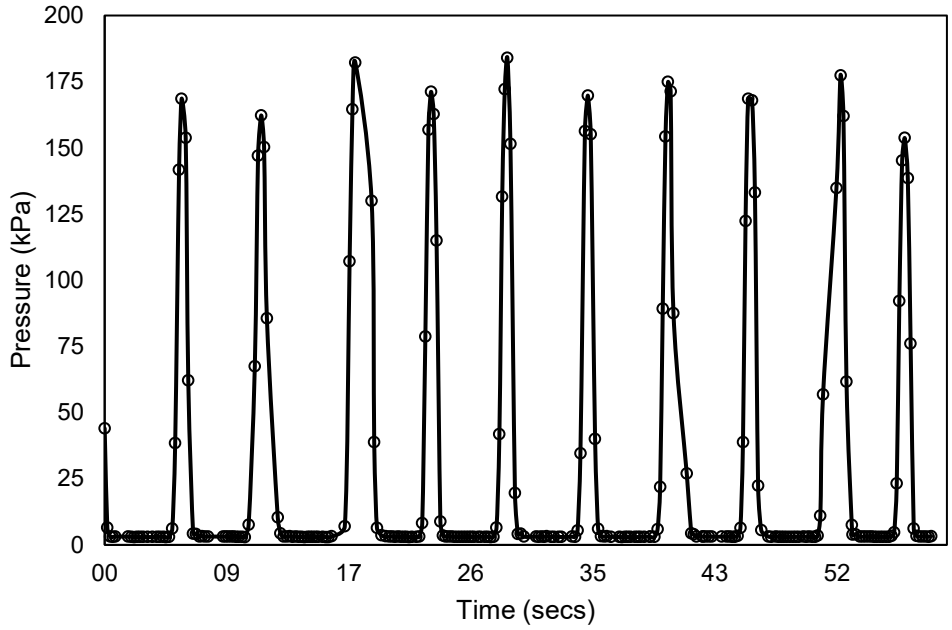

Figure 4.16 Top pressure cell reading taken over a 1-minute period.

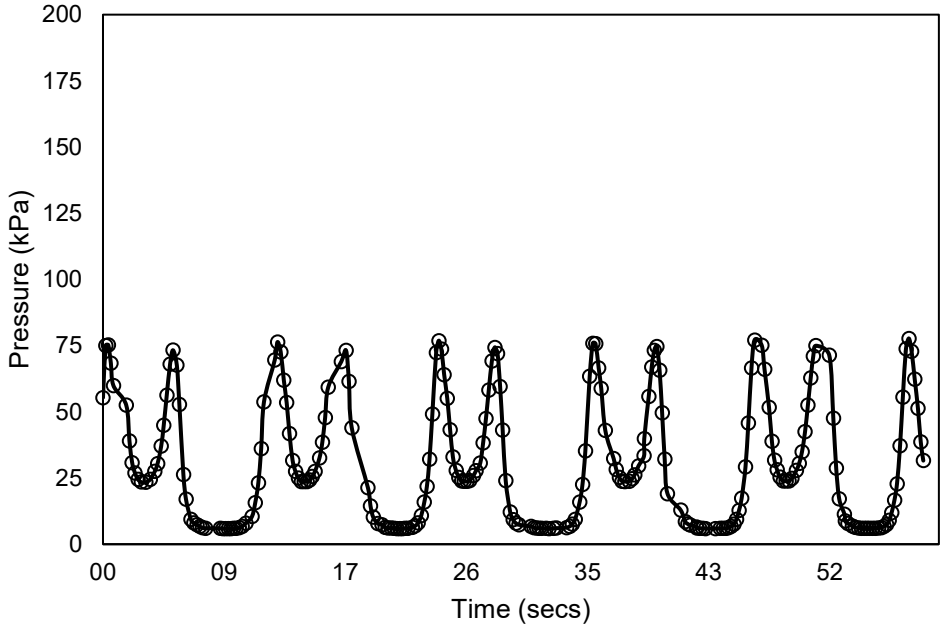

Figure 4.17 Middle pressure cell reading taken over a 1-minute period.

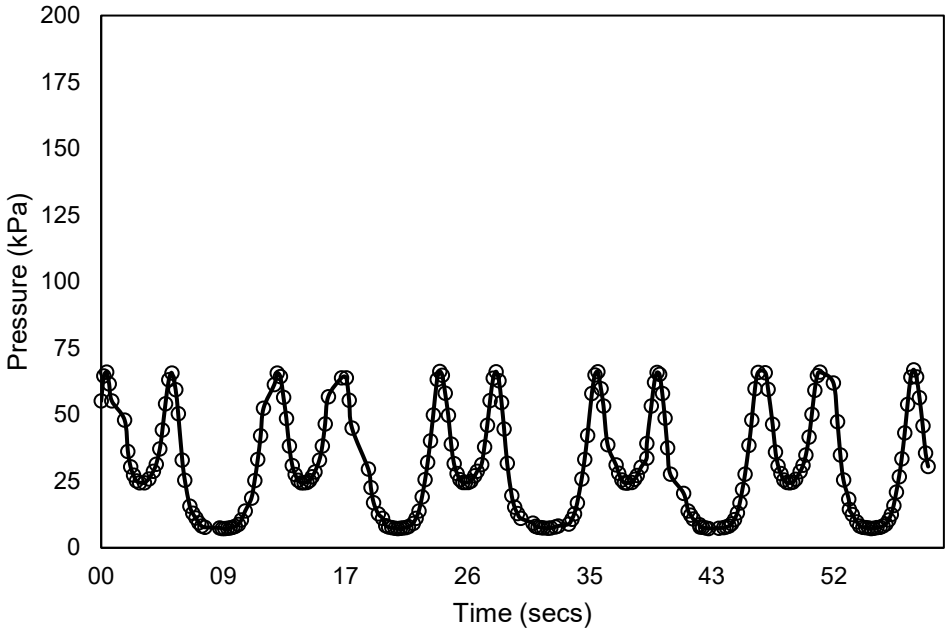

Figure 4.18 Bottom pressure cell reading taken over a 1-minute period.

Table 4.3 Pressure reduction at base/subgrade interface.

Case	Middle Pressure Cell (kPa)	Bottom Pressure cell (kPa)
Control	74	71
GG1 – 12 in	76	66
GG1 – 9 in	118	95

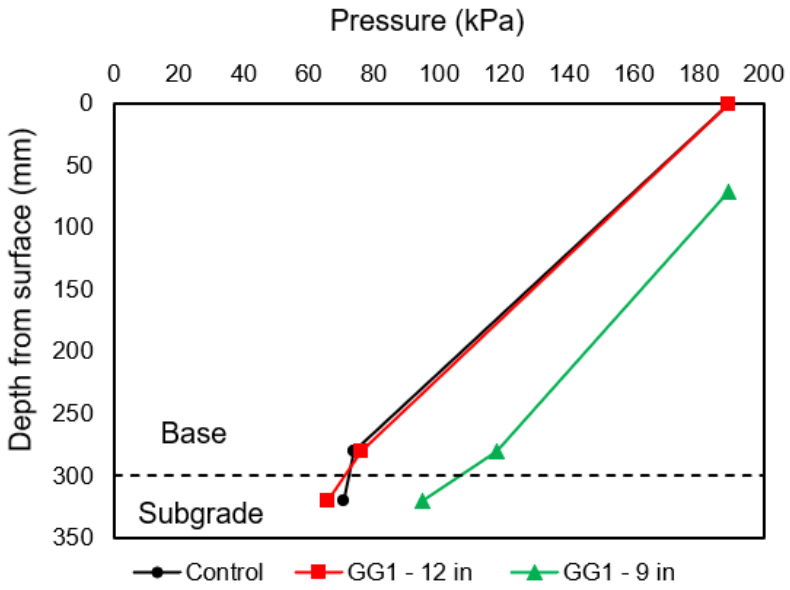

Figure 4.19 Pressure reduction through pavement layer

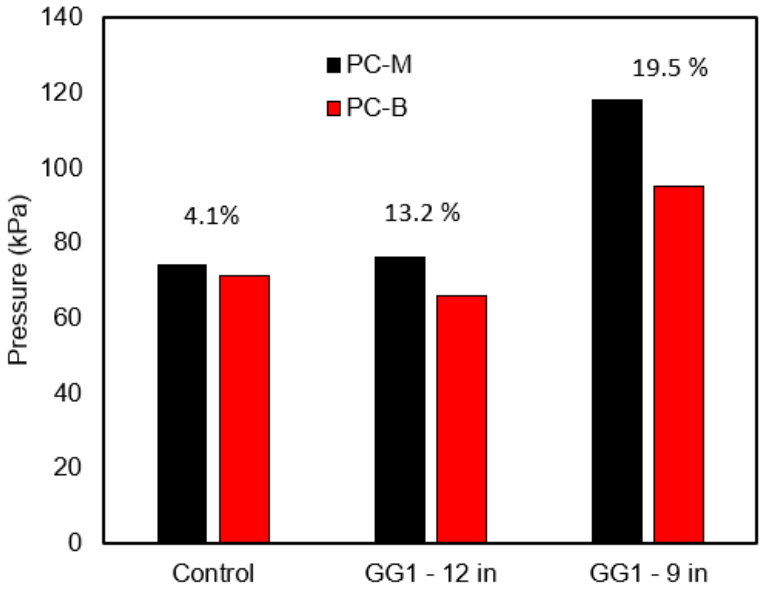

Figure 4.20 Pressure reduction at base/subgrade interface

4.2 Analysis of FLAC Simulations

The simulation was conducted to evaluate the full-scale effect of geosynthetic reinforcement on the response of the pavement layers. Different cases were evaluated for different geosynthetic types and locations. The simulation results were compared to the laboratory test results to confirm the trend and consistency of the outcome. The input parameters for the simulation were obtained from the evaluation of the direct shear and pullout boxes, specifically utilizing the soil-geosynthetic interface, friction angles, and tensile strengths of the geosynthetics.

4.2.1 Modeling setup

Numerical modeling was conducted to investigate the behavior of a typical roadway consisting of asphalt surface layer, aggregate base, and subgrade. The geometric representation of the model is illustrated in **Figure 4.21**. The modeling geometry was based on axi-symmetric conditions, as described by Erickson and Drescher (2001), which allowed us to simulate the

response of the pavement layer without distortion effects from the different axes. A general configuration of the pavement system was adopted, as presented in the literature and the pavement design manual of the Nevada Department of Transportation (NDOT) (NDOT Pavement Design Manual 2021).

The impact of a simulated tandem vehicle load on pavement layer response was investigated as per the Federal Highway Administration (FHWA-HRT-13-091) report (Hallenbeck et al. 2014). To accurately capture the response of the pavement layer near the loading point, we employed a finer mesh in the modeling. The side wall was fixed to ensure boundary conditions that reflect the infinite ground assumption. Additionally, the geostatic condition was considered as the initial state to reflect gravity in the modelling. This approach aligns with previous studies that have used finite element analysis to model pavement layer response subjected to vehicle loading (e.g., Zhang et al. 2017; Sajjadi et al. 2019). The FHWA-HRT-13-091 report is also consistent with other studies that focused on simulating vehicle loads on pavement layers (e.g., Wasiuddin et al. 2017; Saleh et al. 2021).

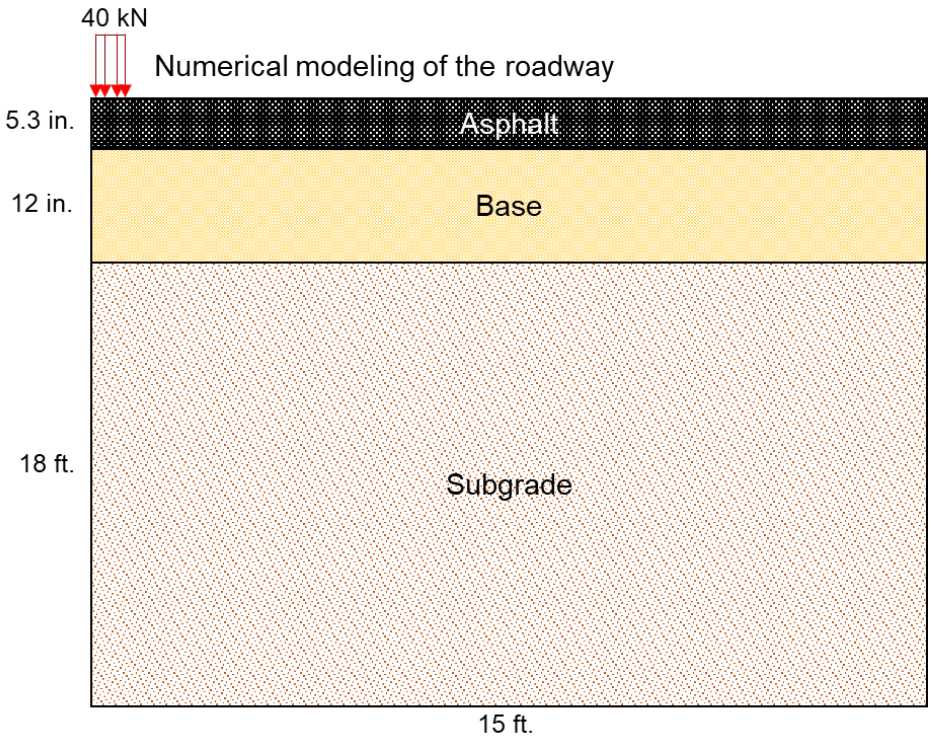

Figure 4.21 Modeling geometric condition.

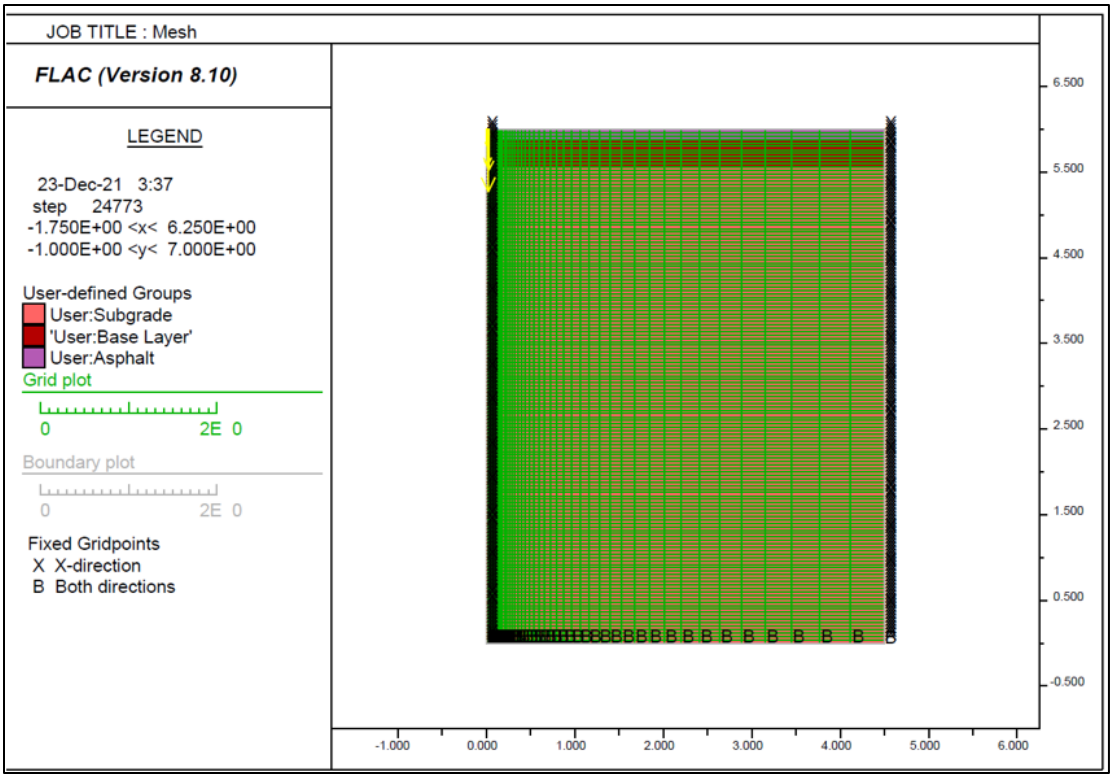

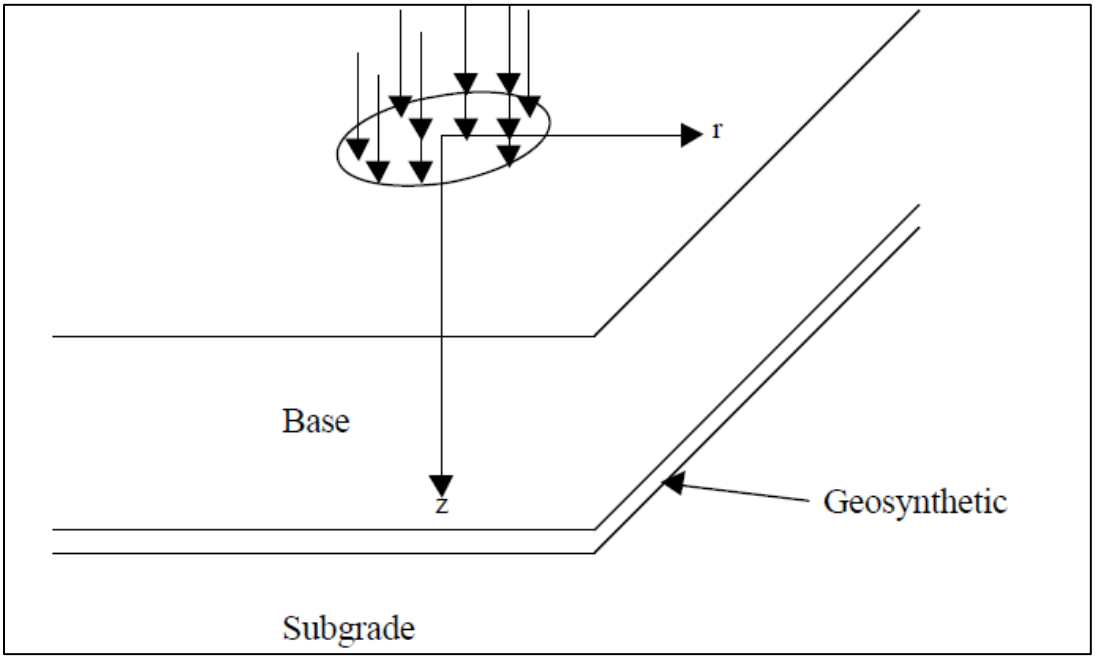

Figure 4.22 Modeling mesh and simulation condition - axisymmetric problem (Erickson and Drescher, 2001

In this study, the modeling parameters for simulating the interface behavior between geosynthetic and soil layers were obtained from both literature and the current investigation. These parameters are listed in **Table 4.4**. To ensure accurate simulation results, the interface properties were calibrated based on the pullout test data. A comparison was made between the modeling and testing results to parameterize the interface properties listed in **Table 4.5**. Among these properties, the bond stiffness and bond friction angle were calibrated with the pullout testing data. The properties were then defined to fit the modeling results to the testing results. Finally, the properties were used for simulating the pavement layer behavior. The methodology used in this study is consistent with similar studies in the field. The calibration of interface properties with pullout testing data has been widely used in pavement engineering (e.g., Wang et al. 2002; Xiao et al. 2019). Additionally, the use of modeling parameters obtained from literature and experimentation is a common practice in engineering simulations (e.g., Han et al. 2018; Zhang et al. 2021).

Table 4.4 Material properties to input the numerical model of each pavement layer

Parameter	**Material**		
	Asphalt [(1)]	**Base layer [(2)]**	**Sand [(3,4)]**
Modulus of Elasticity	174.05×10^3	4786	7251
Soil density (pcf)	143.5	133	111
Poisson's ratio (-)	0.25	0.3	0.25
Cohesion (psi)	0	0	0
Friction angle (deg)	0	65	30
Dilatancy angle (deg)	-	6	0

References :[(1)] Tan et al. (2017), [(2)] Karpurapu et al. (2014), [(3)]Hatami and Bathurst, [(4)]NDOT,

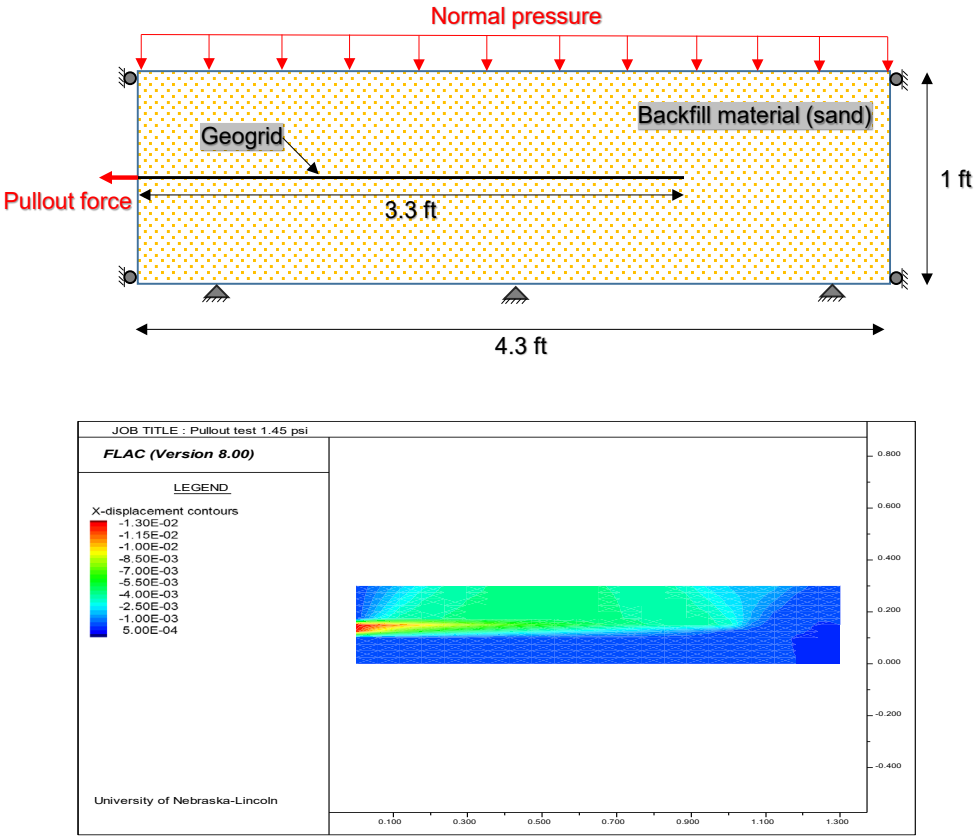

Figure 4.23 Modeling schematic and FLAC modeling example.

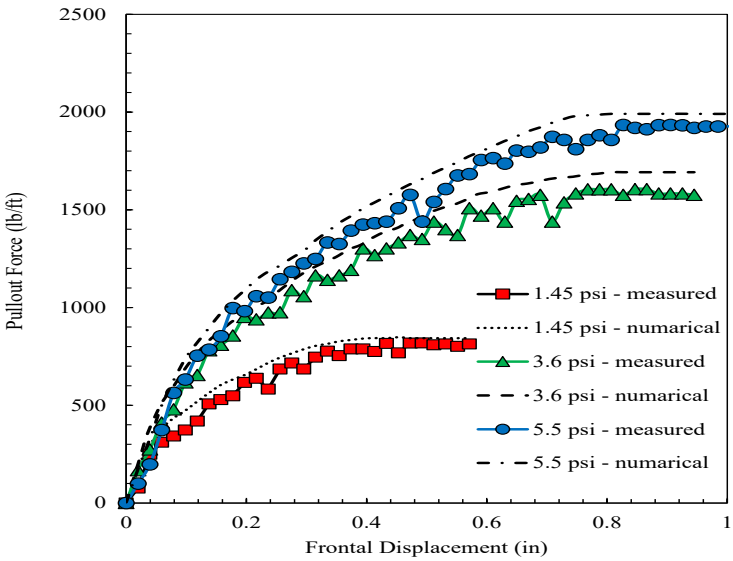

Figure 4.24 Match between pullout testing data and numerical simulation for parameter calibration.

Table 4.5. Parameter for geosynthetic soil composite

Parameter	Biaxial geogrid	Triaxial geogrid	Geotextile
Elasticity modulus (psi)	150×10^3	120×10^3	70×10^3
Bond stiffness, kbond (psf)	36,600	33,400	20,000
Bond friction angle, sfriction (°)	43	39	30
Bond strength, sbond (lb/ft)	560	450	320

* Modified after Abdi and Arjomand (2011) and experimental direct shear tests

4.2.2 Simulation Cases

A series of simulations were conducted to evaluate the effect of the integration of geosynthetic reinforcement sand subgrades. Also, different locations of geosynthetic within the different pavement layers were analyzed. These include geosynthetic reinforcement beneath the asphalt surface layer, middle of base layer and interface between base and subgrade layers. The various cases are evaluated as shown in **Figure 4.25**. A summary of the description of the modelled cases for different soil types are highlighted in **Table 4.6**.

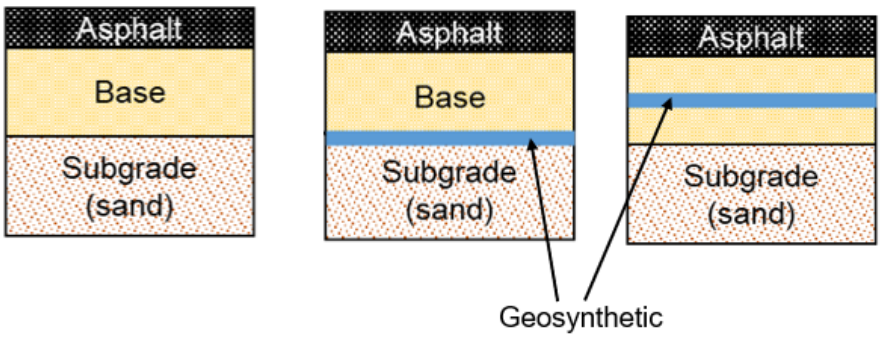

Figure 4.25 Simulation cases.

Table 4.6. Number of simulation cases.

Soil type (subgrade)	Cases modeled	Number of cases
Sand	Change in reinforcement type	4
	Change in reinforcement location	2

4.2.2.1 Simulation Results for Reinforcement in Sand

Figure 4.26 shows the surface displacement or settlement for sand from the center of the point of application of the load along the horizontal distance of the pavement model. The modeling results showed that the displacement was highest for the unreinforced case, followed by the geotextile, triaxial, and biaxial geogrids. While the direct shear tests showed that the geotextile performs poorly in sand, the simulations concluded that geotextile has a better performance than the unreinforced case. This was presumed to be because the geotextile was not subjected to resistive shear and was subjected to more bearing load. In the sand-based test, the geotextile with the lowest confinement increased its performance by 9.02% compared to the unreinforced case. The biaxial geogrid showed an 18.0% reduction in settlement in the simulation while the triaxial geogrid showed a 14.8% reduction in the settlement. The simulations showed that for sand conditions, the biaxial was better than the triaxial with the geotextile showing the least reduction in settlement amongst other evaluated geosynthetic types, which is consistent with the collected data.

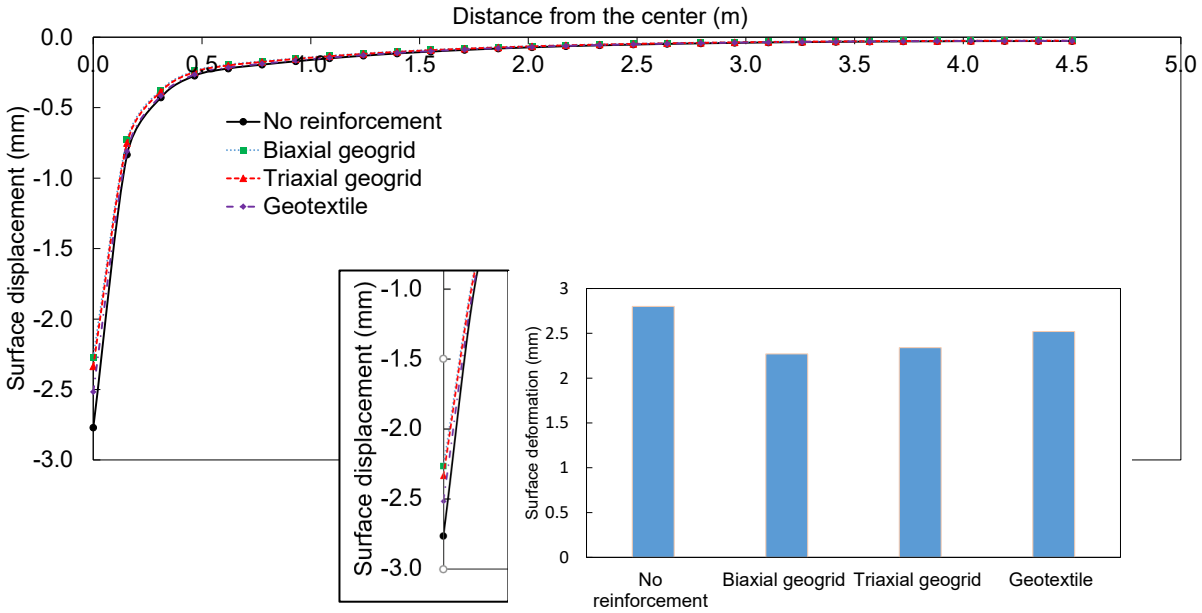

Figure 4.26 Displacement in sand.

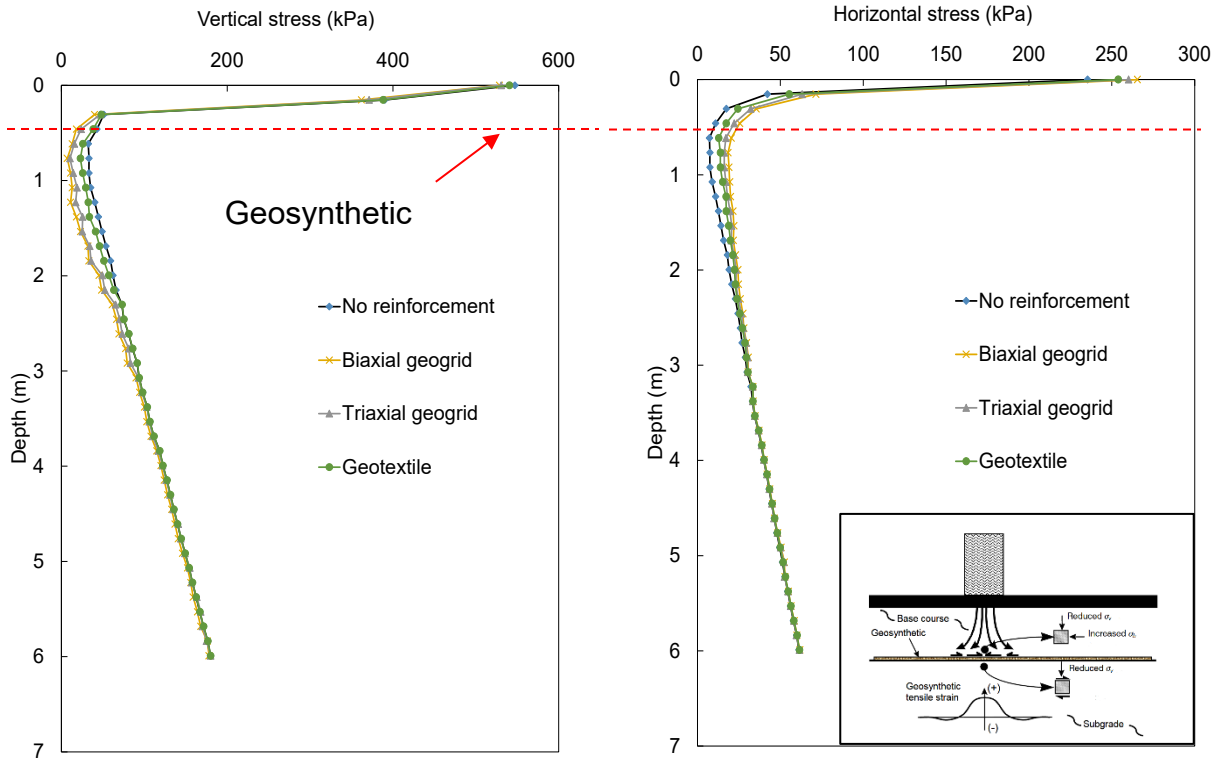

Figure 4.27 Vertical and horizontal stress in sand.

Figure 4.27 shows the vertical and horizontal stresses as a function of depth. The axial loading applied on the surface significantly reduced across the base layer. At the base and subgrade interface, there is a stress dispersion due to the reinforcement. This is because the stress is transferred through the geosynthetic reinforcement reducing its intensity on the underlying subgrade. In the foundation aggregate, the horizontal stresses also increased with the reinforcement layer compared to the case without reinforcement. The case of no reinforcement shows the highest vertical and lowest horizontal stress. The biaxial and triaxial geogrid cases show relatively lower vertical and higher horizontal stress than other cases. The findings indicate a strong correlation between the reinforcement effect and the settlement outcomes. The stress transfer distribution across the pavement layer is highlighted in **Figure 4.27.** This result confirms the significant role geosynthetic plays in reinforcing the pavement layers.

4.2.2.2 Simulation Results for Sand Subgrade-Different Reinforcement Location

The effect of different geosynthetic locations on the response of the pavement layers in the model was evaluated. **Figure 4.28** shows the surface displacement or settlement for different geosynthetic locations within the pavement layers. All three cases showed better performances in reducing the settlement compared to no reinforcement. The settlement observed for the three cases of geosynthetic were comparable with the interface between the base and subgrade layers, showing the least value of settlement. This result could differ from one soil type to another.

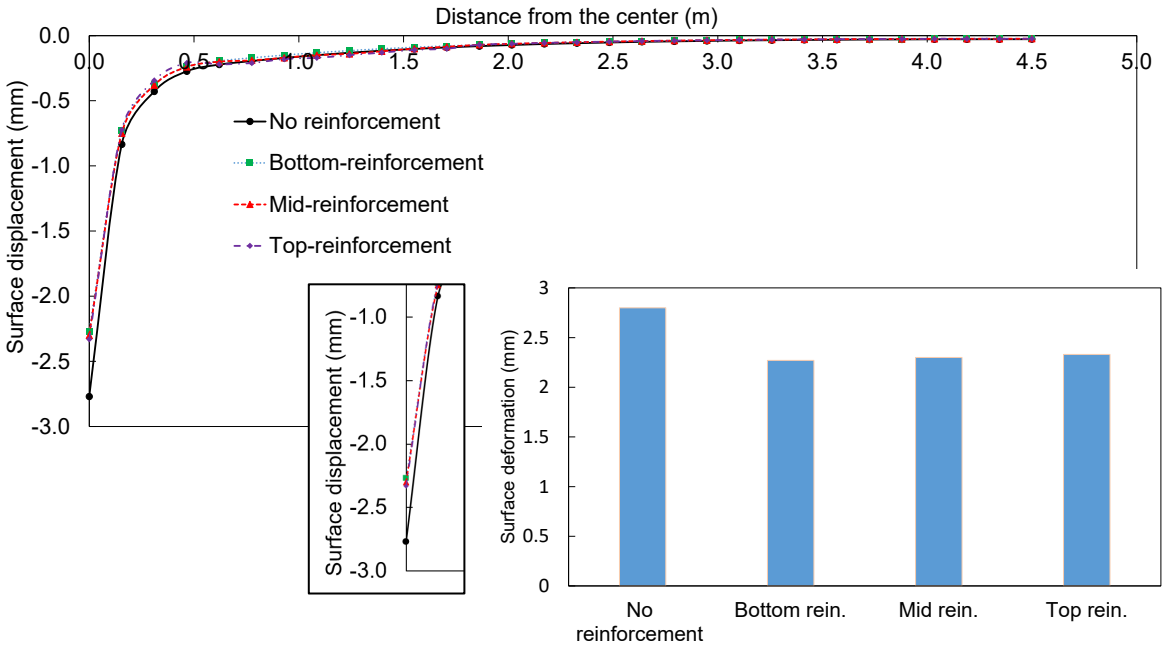

Figure 4.28 Displacement for different location of geosynthetics.

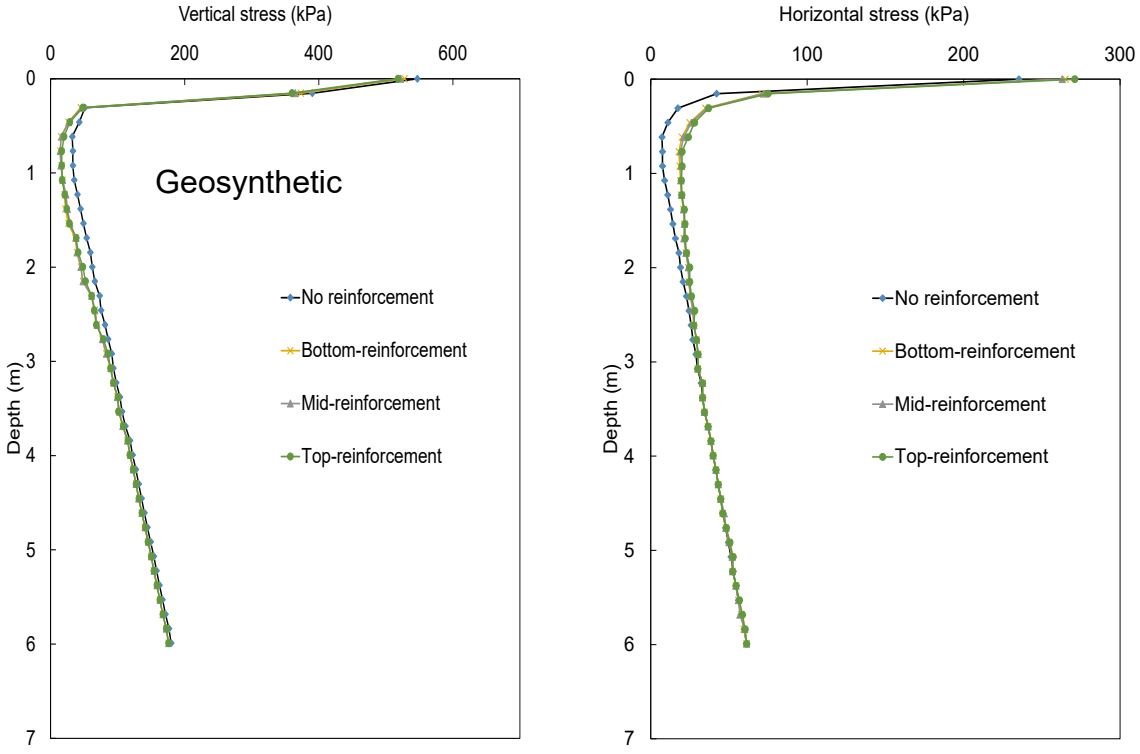

Figure 4.29 Vertical and horizontal stress for different location of geosynthetics.

Similar to other cases, **Figure 4.29** shows the vertical and horizontal stresses as a function of depth when the geosynthetics are installed at different depths. The axial load applied on the surface significantly reduced across the base layer. At the base and subgrade interlayers, there is a stress dispersion due to the geosynthetic reinforcing effect. Similar to the settlement analysis, all three geosynthetic reinforced cases show similar vertical and horizontal stresses.

Chapter 5 Conclusion

This study evaluates the performance of the geosynthetic reinforced roadway pavement layers. Several states in the United States have used geosynthetics to help rehabilitate and elongate the life of subgrades. They are more formally used to protect against underlying damage by stabilizing the subgrade and base layers under the flexible pavement. The benefits of the geosynthetic application includes longer serviceability and slower deterioration. However, the geosynthetic application should be a case-by-case study because of the variable site conditions and soil types. Thus, in this study, extensive experimental work through a Large-Scale Tracking Wheel Test (LSTW) was performed to evaluate various parameters and the performance of the geosynthetic reinforcement for sand subgrade. The parameters include Dynamic Cone Penetrometer Index (DPI), strength/stiffness improvement, deformation reduction and pressure reduction effects and were analyzed to compare performances of reinforced and unreinforced sections.

The use of biaxial geogrid at the subgrade and base interface was effective in reducing the total permanent deformation (rutting) of a pavement system by 34.1% and 29.5% for a 12-in thick base course and a 9-in base, respectively as compared to the control case after the rolling wheel load application. The base's resilient modulus, following the application of rolling wheel loads and using the correlation method established by Lin et al. (2005), exhibited an increase of 30.9% for a 12-inch thick base course and 19.8% for a 9-inch thick base. This increase was in comparison to the control case. The intensity of stress acting on the subgrade layer reduced by 13.2% and 19.5% for a 12-in thick base course and a 9-in base, respectively, as compared to the control case. These results highlight the benefit of using a biaxial geogrid in a pavement layer.

Numerical modeling conducted using FLAC, which incorporated input parameters derived from laboratory tests, was utilized to simulate practical pavement layers both with and without the application of geosynthetics. This simulation demonstrated a significant improvement in reducing settlement and vertical stress when geosynthetics were applied for the cases evaluated. Based on the modeling results, it is found that the stress transfer effect with the use of geosynthetics is clearly generated, and the confined zone of the layer is established, which shows good agreement with DCP data obtained from the LSTW test. The simulation indicated that the optimal placement for geosynthetic installation is at the interface between the base and subgrade. This position proved to be the most effective among other test positions for reducing vertical stress and deformation within the pavement layers.

References

Abdi, M. and Arjomand, M. (2011). “Pullout Tests Conducted on Clay Reinforced with Geogrid Encapsulated in Thin Layers of Sand.” Geotextiles and Geomembranes, 29(6), 588-595.

Abdi, M. and Arjomand, M. (2011). “Pullout Tests Conducted on Clay Reinforced with Geogrid Encapsulated in Thin Layers of Sand.” Geotextiles and Geomembranes, 29(6), 588-595.

Abu-Farsakh, M., Souci, G., Voyiadjis, G.Z., and Chen, Q. (2012). “Evaluation of Factors Affecting the Performance of Geogrid-Reinforced Granular Base Material Using Repeated Load Triaxial Tests.” American Society of Civil Engineers, 24(1), 72-83, https://doi.org/10.1061/(ASCE)MT.1943-5533.0000349.

Adams, C., Apraku, E., and Opoku-Boahen, R. (2015). “Effect of Triaxial Geogrid Reinforcement on CBR Strength of Natural Gravel Soil for Road Pavements.” Journal of Civil Engineering Research, 5(2), 45-51. https://doi.org/10.5923/j.jce.20150502.05.

Al-Qadi, I.L., Dessouky, S., Tutumluer, E., and Kwon, J. “Geogrid Mechanism in Low-Volume Flexible Pavements: Accelerated Testing of Full-Scale Heavily Instrumented Pavement Sections.” International Journal of Pavement Engineering, 121-135, https://doi.org/10.1080/10298436.2010.535534.

Appea, A.K., “In-Situ Behavior of Geosynthetically Stabilized Flexible Pavement,” Virginia Polytechnic Institute and State University, 1997.

Bagshaw, S. A., Herrington, P. R., Kathirgamanathan, P., and Cook-Opus International Consultants LTD, “Geosynthetics in Basecourse Stabilization.” Research Report 574, 2015, Wellington, New Zealand: New Zealand Transportation Agency.

Barksdale, R. D., Brown, S. F., and Chan, F., “Potential Benefits of Geosynthetics in Flexible Pavement Systems,” pp. 56, Transportation Research Record #315, 1989, Washington, D.C.

Barksdale, R. D., Brown, S. F., and Chan, F., “Potential Benefits of Geosynthetics in Flexible Pavement Systems,” pp. 56, Transportation Research Record #315, 1989, Washington, D.C.

Barksdale, R. D., Brown, S. F., and Chan, F., “Potential Benefits of Geosynthetics in Flexible Pavement Systems,” pp. 56, Transportation Research Record #315, 1989, Washington, D.C.

Carmichael, R.F. and Marienfeld, M.L., “Synthesis and Literature Review of Nonwoven Paving Fabrics Performance in Overlays,” pp. 112-124, Transportation Research Record #1687, 1999, Washington, D.C.

Chen, D. H., Lin, D. F., Liau, P. H., and Bilyeu, J. (2005). “A Correlation Between Dynamic Cone Penetrometer Values and Pavement Layer Moduli,” Geotechnical Testing Journal, ASTM International, 28(1), West Conshohocken, Pennsylvania.

Chen, W., Zhou, W., and Jing, X. (2019). “Modeling Geogrid Pullout Behavior in Sand Using Discrete-Element Method and Effect of Tensile Stiffness.” American Society of Civil Engineers, 19(5), 04019039, https://doi.org/10.1061/(ASCE)GM.1943-5622.0001424.

Cuelho, E. and Perkins, S., “Field Investigation of Geosynthetics Used for Subgrade Stabilization,” U.S. Department of Transportation, Federal Highway Administration in cooperation with the State of Montana Department of Transportation, 2009, Report Number: FHWA/MT-09-003/8193.

Ebrahimian, B., “Numerical Analysis of Strip Footing Resting on Geosynthetic-Reinforced Sand Bed Over Soft Soil,” pp. 993-1000, In Deformation Characteristics of Geomaterials, 2011, IOS Press.

El-Maaty, A.E. (2016). “Improving Rutting Resistance of Flexible Pavement Using Geosynthetics.” Open Access Library Journal, 3(5), 1-11. https://doi.org/10.4236/oalib.1102655.

Erickson, H., & Drescher, A. (2001). 4. Title and Subtitle 5. Report Date THE USE OF GEOSYNTHETICS TO REINFORCE LOW VOLUME ROADS.

"Eun, J., Gupta, R., and Zornberg, J.G. (2017). “Effect of Geogrid Geometry on Interface

Resistance in a Pullout Test,” pp. 236-246, ASCE Geo-Frontier, Orlando, Florida. "

"Eun, J., Gupta, R., and Zornberg, J.G. (2017). “Effect of Geogrid Geometry on Interface

Resistance in a Pullout Test,” pp. 236-246, ASCE Geo-Frontier, Orlando, Florida. "

Fannin, R.J. and Sigurdsson, O. (1996). “Field Observations on Stabilization of Unpaved Roads with Geosynthetics.” Journal of Geotechnical Engineering, 122, 544-553, http://dx.doi.org/10.1061/(ASCE)0733-9410(1996)122:7(544).

Giroud, J.P. and Han, J. (2004). “Design Method for Geogrid-Reinforced Unpaved Roads I,” Journal of Geotechnical and Geoenvironmental Engineering, 130(8), 775-786.

Giroud, J.P. and Han, J. (2004). “Design Method for Geogrid-Reinforced Unpaved Roads II,” Journal of Geotechnical and Geoenvironmental Engineering, 130(8), 787-797.

Haliburton, T.A., Fowler, J., and Langan, J.P., “Design and Construction of a Fabric Reinforced Test Section at Pinto Pass, Mobile, Alabama,” Transportation Research Record #79, 1980, Washington, D.C.

Harison, J. A., “In Situ CBR Determination by DCP Testing Using a Laboratory- Based Correlation,” Australian Road Research Board, 19(4), 1986.

Hatami, K. and Bathurst, R. J. “Modeling Static Response of a Segmental Geosynthetic Reinforced Soil Retaining Wall Using FLAC,” pp. 223-231, Proceedings from the 2nd International FLAC Symposium, Numerical Modeling in Geomechanics, 2001, Lyon.

Hatami, K. and Bathurst, R. J. “Modeling Static Response of a Segmental Geosynthetic Reinforced Soil Retaining Wall Using FLAC,” pp. 223-231, Proceedings from the 2nd International FLAC Symposium, Numerical Modeling in Geomechanics, 2001, Lyon.

Holtz, R.D. and Lee, W.F., “Geosynthetic-Reinforced Wall Analysis Phase II: Use of In-Soil Geosynthetic Behavior to Predict Deformations, Volume 2: Implementation — Computer Codes and Files,” 1998, No. WA-RD 452.2.

Holtz, R.D. and Lee, W.F., “Geosynthetic-Reinforced Wall Analysis Phase II: Use of In-Soil Geosynthetic Behavior to Predict Deformations, Volume 2: Implementation — Computer Codes and Files,” 1998, No. WA-RD 452.2.

Holtz, R.D., Christopher, B.R. and Berg, R.R., “Geosynthetic Design and Construction Guidelines,” pp. 460, U.S. Department of Transportation, Federal Highway Administration, 1998, Washington, D.C., FHWA-HI-98-038.

Hoppe, E.J., Hossain, M.S., Moruza, A.K., and Weaver, C.B., “Use of Geosynthetics for Separation and Stabilization in Low-Volume Roadways,” Virginia Transportation Research Council, Report Number: FHWA/VTRC 20-R8.

Imjai, T., Pilakoutas, K., and Guadagnini, M. (2019). “Performance of Geosynthetic-Reinforced Flexible Pavements in Full-Scale Field Trials.” Geotextiles and Geomembranes, 47, 217-229.

Iowa Department of Transportation. “Iowa Statewide Urban Design and Specifications,” 2013, https://iowasudas.org/manuals/design-manual/.

Iowa Department of Transportation. “Standard Specifications for Highway and Bridge Construction,” Iowa Department of Transportation, 2012.

Itasca Consulting Group, Inc. “FLAC: Explicit Continuum Modeling of Non-Linear Material Behavior in 2D.” https://itascacg.com/software/FLAC, Accessed 26 January 2022.

Kaswell, E.R., “Handbook of Industrial Textiles,” West Point Pepperell, 1963, New York, New York.

Kazmee, H., Mishra, D., and Tutumluer, E. “Sustainable Alternatives in Low Volume Road Base Course Applications Evaluated through Accelerated Pavement Testing,” International Foundations Congress and Equipment Expo, pp. 409-418, 2015.

Keller, G.R. (2016). “Application of Geosynthetics on Low-Volume Roads.” Transportation Geotechnics, 8, 119-131.

Kermani, B., Xiao, M., Stoffels, S.M., and Qiu, T. (2018). “Reduction of Subgrade Fines Migration into Subbase of Flexible Pavement Using Geotextile.” Geotextiles and Geomembranes, 46, 377-383.

"Kim, S., Frost, D., Durham, S., Chorzepa, M., Wright, J., and Hanumasagar, S. (2018). "Development of Geosynthetic Design and Construction Guidelines for Pavement Embankment Construction in North Georgia." FHWA-GA-19-1611,

Georgia Department of Transportation. "

Koerner, R. M. (2005). "Designing with Geosynthetics, 2nd Edition," Pearson Prentice Hall, New Jersey.

Koerner, R.M. (2012). "Designing with Geosynthetics, 6th Edition," Xlibris Corporation, 1(2).

Lambe, T.W. and Whitman, R. V. (1969). "Soil Mechanics," Wiley and Sons, New York, New York.

Latha, G.M. and Nair, A.M. (2014). "Geosynthetics in Unpaved Roads," Indian Journal of Geosynthetics and Ground Improvement, 3(2), 3-13.

Leng, J. and Gabr, M.A. (2005). "Numerical Analysis of Stress-Deformation Response in Reinforced Unpaved Road Sections," Geosynthetics International, 12, 111-119, http://dx.doi.org/10.1680/gein.2005.12.2.111.

Miura, N., Sakai, A., Taesiri, Y., Yamanouchi, T., and Yasuhara, K. (1990). "Polymer Grid Reinforced Pavement on Soft Clay Grounds." Geotextiles and Geomembranes, 9(1), 99-123, https://doi.org/10.1016/0266-1144(90)90007-Y.

Mohammad, L.N., Herath, A., Gudishala, R., Nazzal, D., Abu-Farsakh, M.Y., and Alshibli, K., "Development of Models to Estimate the Subgrade and Subbase Layers' Resilient Modulus from In-Situ Devices: Test Results for Construction Control," Louisiana Transportation Research Center, 2008.

Motanelli, F., Zhao, A., and Rimoldi, P. (1997). "Geosynthetics-Reinforced Pavement System: Testing and Design." Proceedings of Geosynthetics, 97, 549-604.

Mounes, S.M., Karim, M.R., Mahrez, A., and Khodaii, A. (2011). "An Overview on the Use of Geosynthetics in Pavement Structures." Scientific Research and Essays, 6(11), 2234-2241, https://doi.org/10.5897/SRE10.960.

Muhmood, L., Abdu, A., and Khudhur, R.M. (2021). "Using Geotextile to Reduce the Required Thickness of Subbase Layer of the Road and Improvement in CBR Value." Journal of Physics: Conference Series, 1973(1), 1-14, https:// doi.org/10.1088/1742-6596/1973/1/012120.

Myles, B. and Carswell, I. (1986). "Tensile Testing of Geotextiles," pp. 713-718, Proceedings on the 3rd International Conference on Geotextiles, Vienna, Austria.

Nunn, M.E. (1998). "Structural Design of Long-Life Flexible Roads for Heavy Traffic." Proceedings of the Institution of Civil Engineers – Transportation, 129(3), 126-133, https://doi.org/10.1680/itran.1998.30858.

Oliver, T., Wayne, M., and Kwon, J. (2016). “Mechanical Stabilization of Unbound Layers to Increase Pavement Performance and Incorporation of Benefits into M-E Analysis,” Procedia Engineering: Advances in Transportation Geotechnics, The 3rd International Conference on Transportation Geotechnics, 143, 896-910.

Perkins, S.W., Bowders, J.J., Christopher, B.R., and Berg, R.R. (2005). “Geosynthetic Reinforcement for Pavement Systems: US Perspectives,” pp. 1-25, ASCE Geo-Frontier, Austin, Texas.

"Radhakrishna, H. S. and Klym, T. W. (1974). “Geotechnical Properties of a Very Dense Glacial Till.” Canadian Geotechnical Journal, 11(3), 396-408.

Rahman, M.A., Arulrajah, A., Piratheepan, J., Bo, M.W., and Imteaz, M.A. (2014). “Resilient Modulus and Permanent Deformation Responses of Geogrid-Reinforced Construction and Demolition Materials.” American Society of Civil Engineers, 26(3), 512-519, https://doi.org/10.1061/(ASCE)MT.1943-5533.0000824.

Rajagopal, K., Chandramouli, S., Parayil, A., and Iniyan, K. (2014). “Studies on Geosynthetic-Reinforced Road Pavement Structures.” International Journal of Geotechnical Engineering, 8(3), 287-298.

Shukla, S.K. and Yin, J., “Fundamentals of Geosynthetic Engineering,” Taylor and Francis, 2006

Song, C. R., Chung, R. M., Bahmyari, H., and Bitar, L. (2018). “Nebraska Specific Slope Design Manual,” Nebraska Department of Transportation, NDOT: SPR-1 (17) M061, NTC: 26-1121-4036-001).

Steward, J.E., Williamson, R., and Mohney, J., “Guidelines for Use of Fabrics in Construction and Maintenance of Low-Volume Roads,” pp. 172, USDA Forest Service Report PB-276 972, 1977, Portland, Oregon.

Subramanian, N., “Design of Steel Structures,” Oxford University Press, 2008.

Sun, X., Han, J., Kwon, J., Parsons, R. L., & Wayne, M. H. (2015). Radial stresses and resilient deformations of geogrid-stabilized unpaved roads under cyclic plate loading tests. Geotextiles and Geomembranes, 43(5), 440–449. https://doi.org/10.1016/j.geotexmem.2015.04.018

Tan, Y., Sun, Z., Gong, X., Xu, H., Zhang, L., and Bi, Y. (2017). “Design Parameter of Low Temperature Performance for Asphalt Mixtures in Cold Regions.” Construction and Building Materials, 155, 1179-1187.

Tensar International Corporation, “Accelerated Pavement Testing with Tensar Triaxial Geogrids,” Tensar International Corporation, 2017, Tensar Information Bulletin, IB/Accelerated Pavement Testing.

Tingle, J.S. and Jersey, S.R., “Cyclic Plate Load Testing of Geosynthetic-Reinforced Unbound Aggregate Roads,” pp. 60-69, Transportation Research Record, 1936(1), 2005, Washington, D.C.

Vulova, C. and Leshchinsky, D., "Effects of Geosynthetic Reinforcement Spacing on the Behavior of Mechanically Stabilized Earth Walls," Federal Highway Administration, Office of Infrastructure Research and Development, 2003, No. FHWA-RD-03-048.

Wang, Z. and Richwien, W. (2002). "A Study of Soil-Reinforcement Interface Friction." Journal of Geotechnical and Geoenvironmental Engineering, 128(1), 92-94.

Wasage, T.L., Ong, G.P., Fwa, T.F., and Tan, S.A. (2004). "Laboratory Evaluation of Rutting Resistance of Geosynthetics Reinforced Asphalt Pavement." Journal of the Institute of Engineers, 1(2), 29-44.

Webster, S. L., Grau, R. H., and Williams, T. P., "Description and Application of Dual Mass Dynamic Cone Penetrometer," U.S. Army Engineer Research and Development Center, Waterways Experiment Station, Instruction Rep. GL-92-3, Vicksburg, Mississippi, 1992.

Webster, S.L., "Geogrid Reinforced Base Courses for Flexible Pavements for Light Aircraft: Test Section Construction, Behavior Under Traffic, Laboratory Tests, and Design Criteria," Federal Aviation Administration Technical Report GL-93-6, 1993.

Yoder, E.J. and Witczak, M.W. (1975). "Principles of Pavement Design, 2nd Edition," pp. 711, Wiley and Company, London, England.

Zheng, Y. and Fox, P.J. (2017). "Numerical Investigation of the Geosynthetic-Reinforced Soil-Integrated Bridge System Under Static Loading." Journal of Geotechnical and Geoenvironmental Engineering, 143(6), 04017008.

Zheng, Y., Fox, P. J., and Shing, P. B. (2014). "Numerical Simulations for Response of MSE Wall-Supported Bridge Abutments to Vertical Load." In-Ground Improvement and Geosynthetics, 493-502.

Zheng, Y., Fox, P. J., and Shing, P. B. (2014). "Numerical Simulations for Response of MSE Wall-Supported Bridge Abutments to Vertical Load." In-Ground Improvement and Geosynthetics, 493-502.

Zheng, Y., Fox, P. J., and Shing, P. B. (2014). "Numerical Simulations for Response of MSE Wall-Supported Bridge Abutments to Vertical Load." In-Ground Improvement and Geosynthetics, 493-502.

Zofka, A., Zofka, E., Maliszewski, M., and Zalimiene, L. (2017). "Geogrid Reinforcement of Asphalt Pavements." The Baltic Journal of Road and Bridge Engineering, 12(3), 181-186. https://doi.org/10.3846/bjrbe.2017.22.

Zornberg, J.G. (2017). "Functions and Applications of Geosynthetics in Roadways." Procedia Engineering, 189, 298-306, https://doi.org/10.1016/j.proeng.2017.05.048.

Zornberg, J.G. (2017). "Functions and Applications of Geosynthetics in Roadways." Procedia Engineering, 189, 298-306, https://doi.org/10.1016/j.proeng.2017.05.048.

Zornberg, J.G. (2017). “Functions and Applications of Geosynthetics in Roadways.” Procedia Engineering, 189, 298-306, https://doi.org/10.1016/j.proeng.2017.05.048.

Zornberg, J.G. and Gupta, R. (2010). “Geosynthetics in Pavements: North American Contributions,” 1, pp. 379-400, Proceedings on the 9th International Conference on Geosynthetics, Guaruja, Brazil.

Zornberg, J.G. and Gupta, R. (2010). “Geosynthetics in Pavements: North American Contributions,” 1, pp. 379-400, Proceedings on the 9th International Conference on Geosynthetics, Guaruja, Brazil.

Zumrawi, M. and Abdalgadir, E. (2019). "Experimental Study of Geotextile Effect on Bearing Strength and Permeability of Sudanese Cohesive Soils.” University of Khartoum Engineering Journal, 9(1), 21-26.

Appendix – The Large-Scale Tracking Wheel Test Drawings

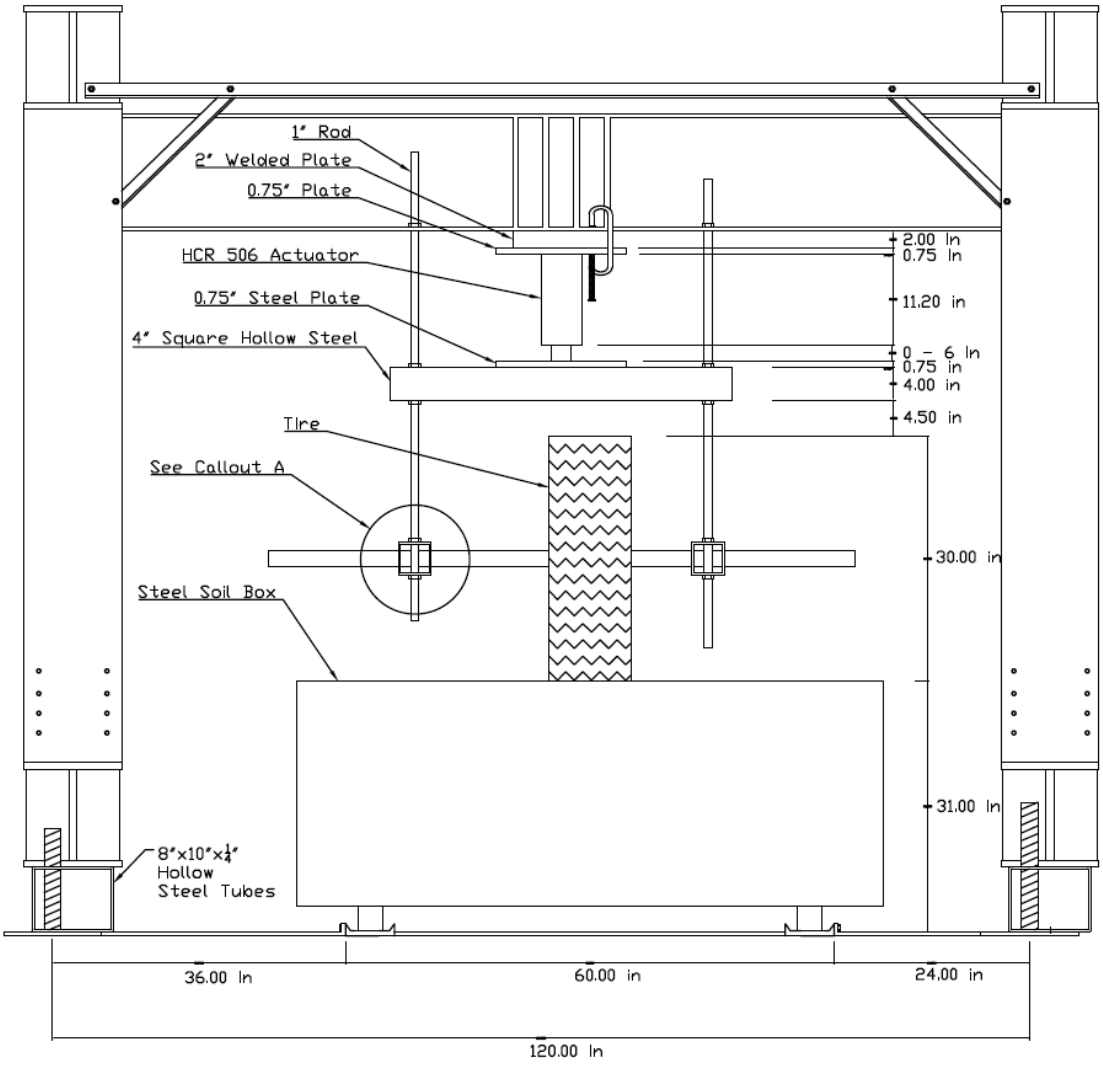

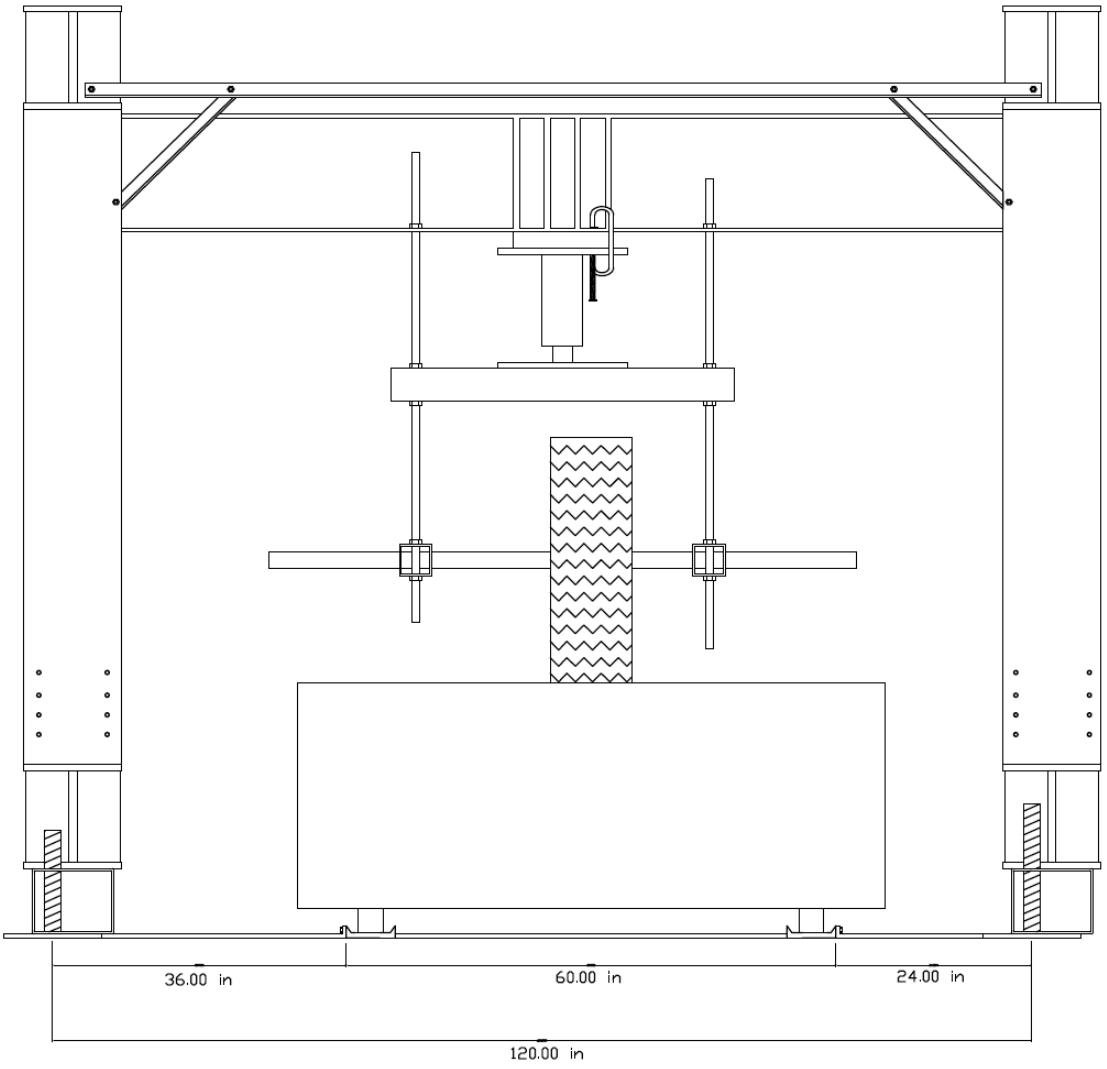
36.00 in
60.00 in
24.00 in
120.00 in

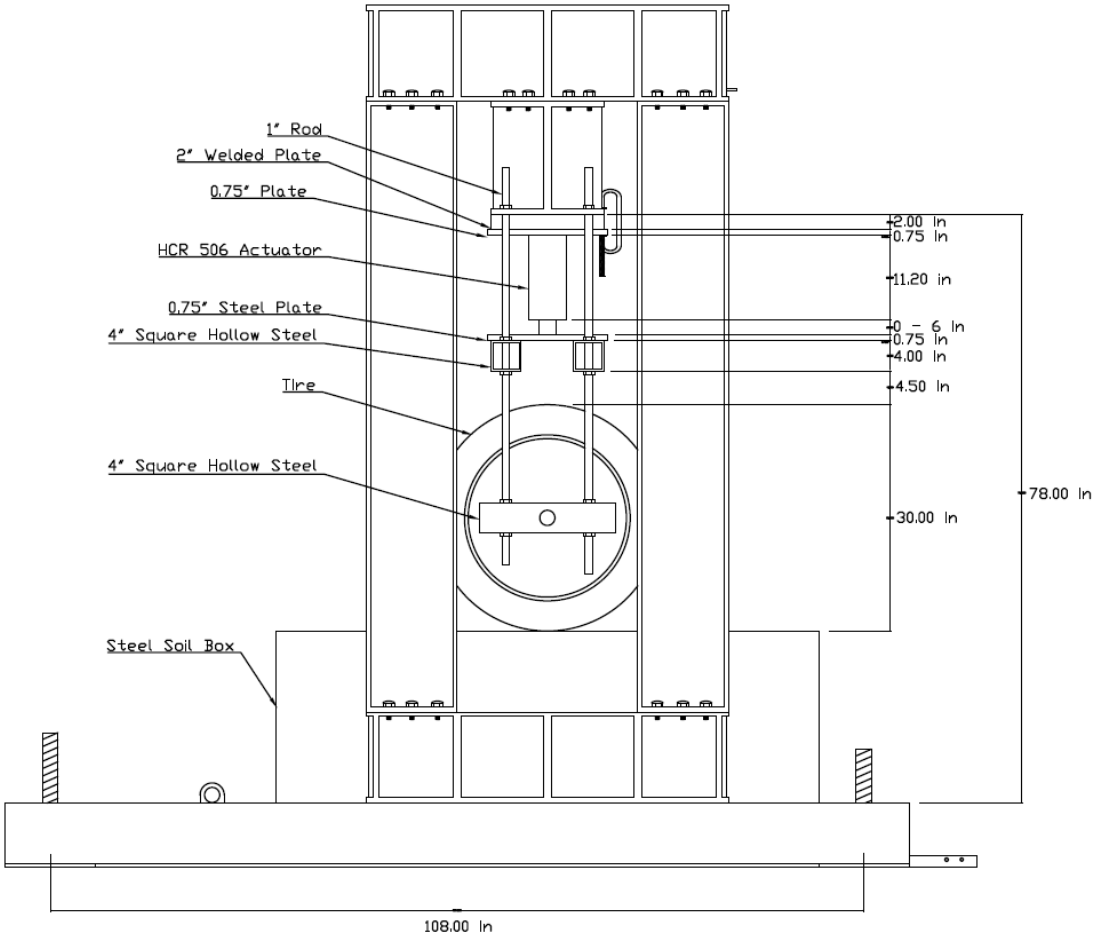
1" Rod
2" Welded Plate
0.75" Plate
HCR 506 Actuator
0.75" Steel Plate
4" Square Hollow Steel
Tire
4" Square Hollow Steel
Steel Soil Box
2.00 in
0.75 in
11.20 in
0 - 6 in
0.75 in
4.00 in
4.50 in
30.00 in
78.00 in
108.00 in

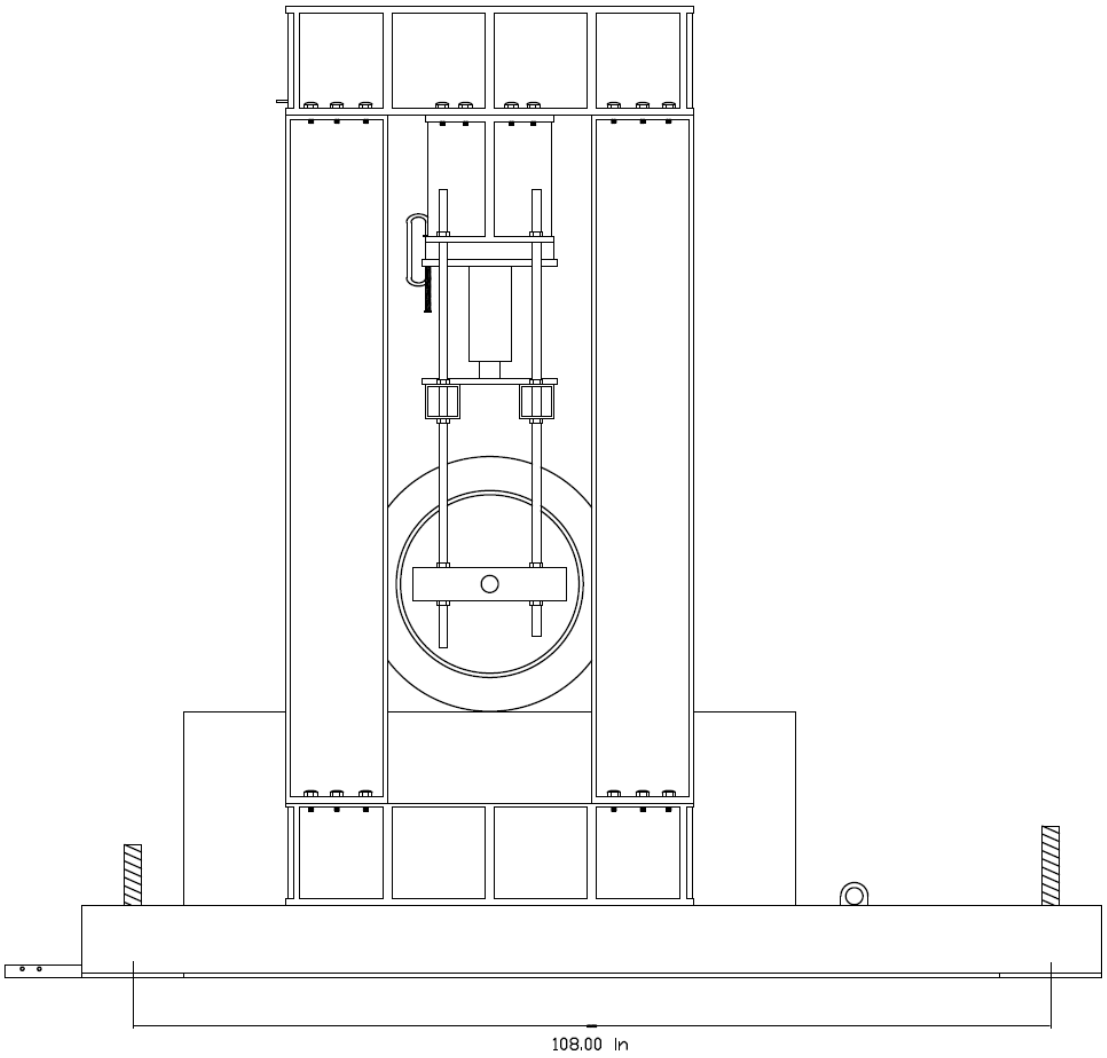
108.00 In

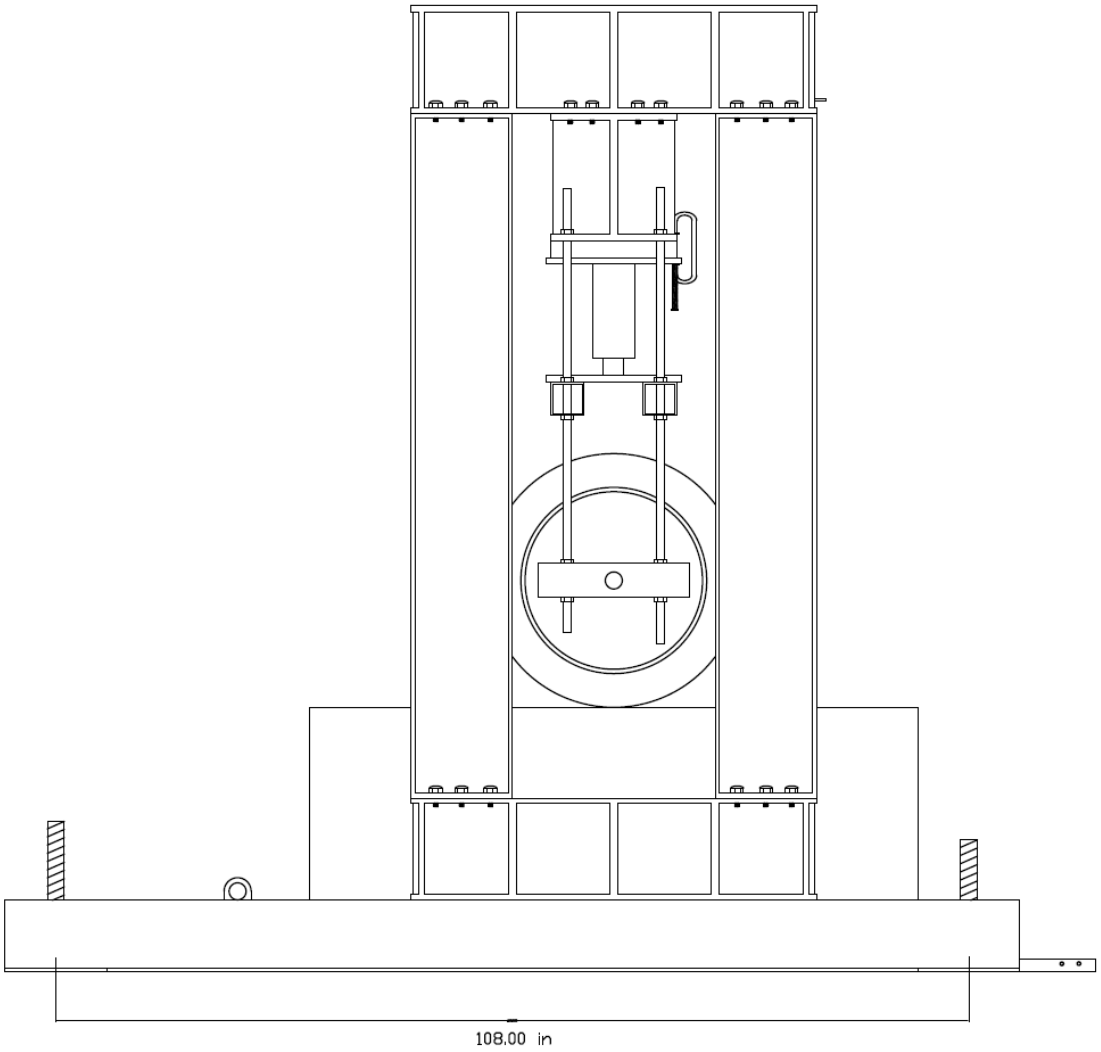
108.00 in

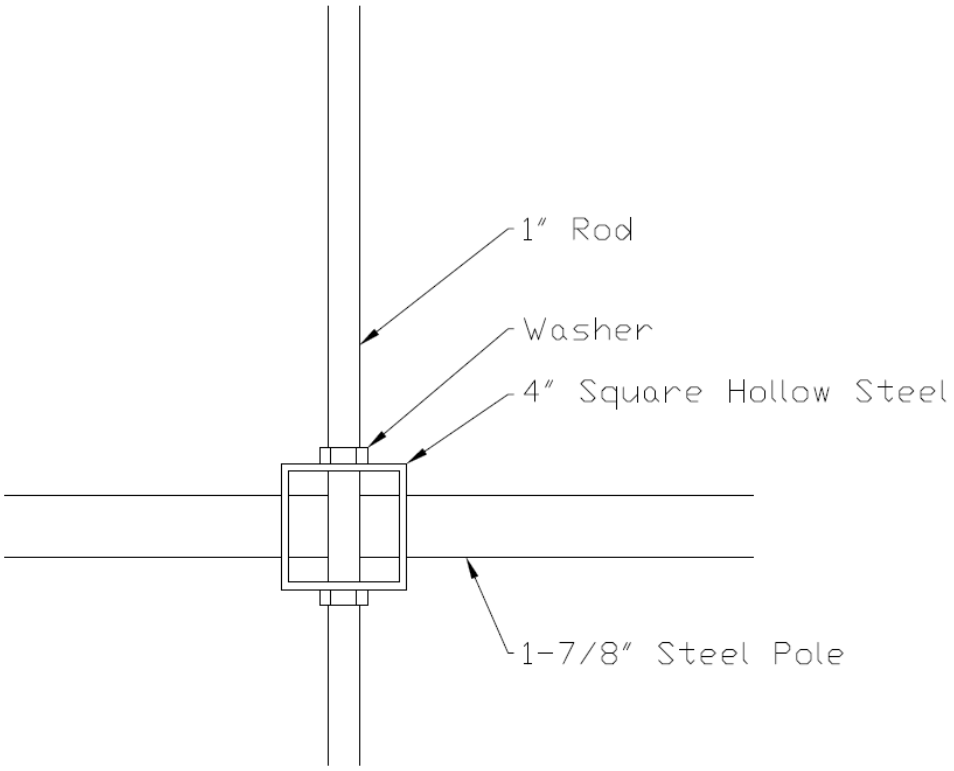

Callout A


108.00 in
36.00 in
60.00 in
24.00 in

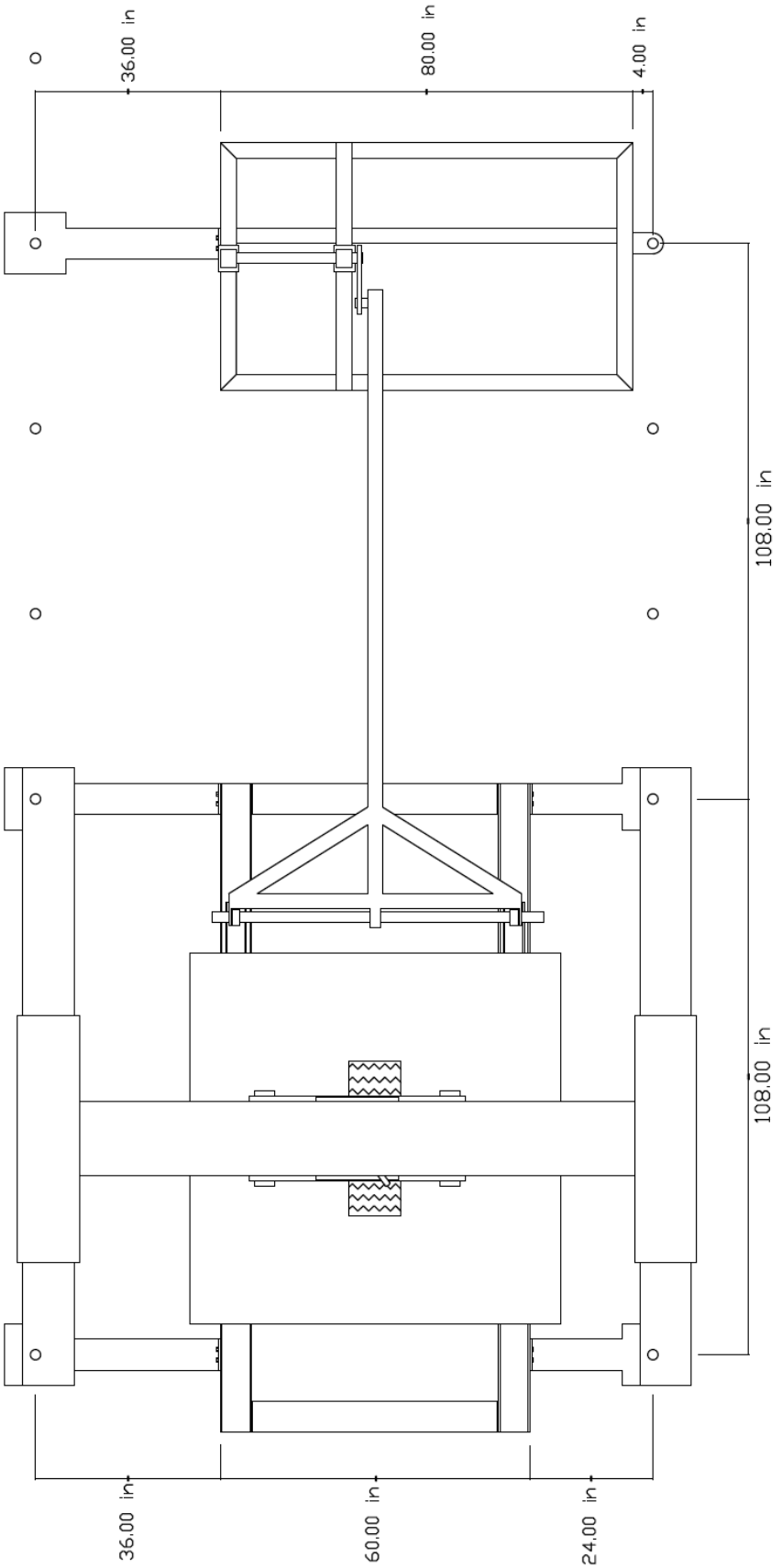
36.00 in
80.00 in
4.00 in
108.00 in
108.00 in
36.00 in
60.00 in
24.00 in

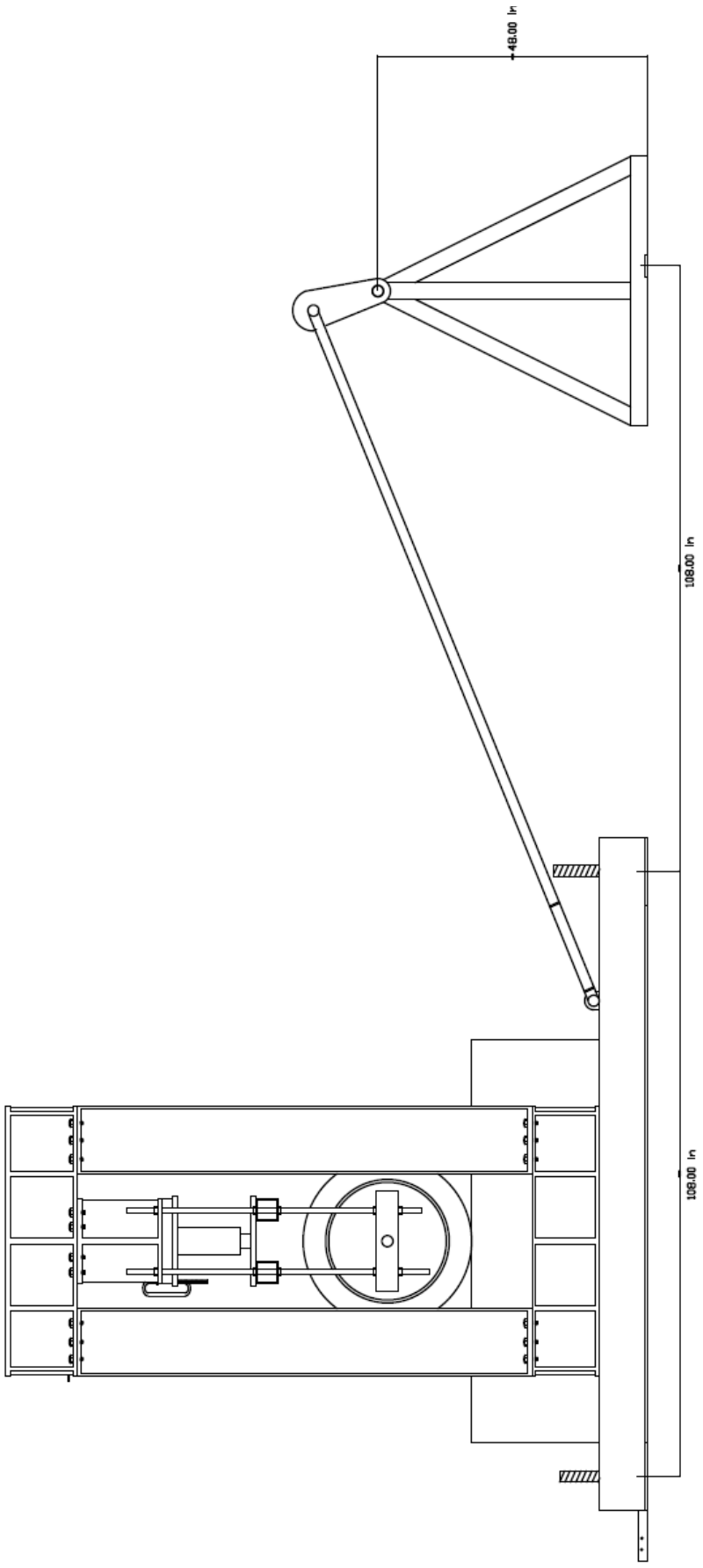
48.00 in
108.00 in
108.00 in